# Effects of bedrock groundwater on spatial and temporal variations in soil mantle groundwater in a steep granitic headwater catchment

Shin'ya Katsura,[1] Ken'ichirou Kosugi,[1] Tasuku Mizutani,[1] Suemi Okunaka,[1] and Takahisa Mizuyama[1]

Received 23 October 2007; revised 5 June 2008; accepted 17 July 2008; published 23 September 2008.

[1] We investigated processes of soil mantle groundwater generation in a granitic headwater catchment in central Japan. Two types of groundwater were observed: ephemeral-type groundwater (EG), which developed in response to rainfall events and disappeared rapidly after the events ceased, and semiperennial-type groundwater (SPG), which remained formed for more than several months. The groundwater level, chemistry, and temperature within the soil and bedrock layers indicated that the source of EG was rain or soil water, whereas the source of SPG was deep bedrock groundwater. The generation processes of soil mantle groundwater varied both spatially and temporally under the influence of the underlying bedrock. Whereas only EG was generated in upslope areas, bedrock groundwater continuously seeped into the soil layers in downslope areas to generate SPG. In middle-slope areas, an increase in the bedrock groundwater level generated SPG in soil layers, but the SPG disappeared when the bedrock groundwater level fell. Our results indicate that bedrock is important in controlling soil mantle groundwater generation and water flow processes in headwater catchments and that direct measurements of bedrock conditions are vital for clarifying the roles of bedrock in these processes.

**Citation:** Katsura, S., K. Kosugi, T. Mizutani, S. Okunaka, and T. Mizuyama (2008), Effects of bedrock groundwater on spatial and temporal variations in soil mantle groundwater in a steep granitic headwater catchment, *Water Resour. Res.*, *44*, W09430, doi:10.1029/2007WR006610.

## 1. Introduction

[2] How rainwater delivered to headwater catchments is discharged into streams has received much research interest and is an important topic in hydrology. Especially since the 1960s, increasing attention has been paid to subsurface flow as a dominant process for runoff generation in humid, soil-mantled, and vegetated catchments. Detailed observations have been carried out at various study sites, including the Maimai catchment, New Zealand [*Mosley*, 1979, 1982; *Sklash et al.*, 1986; *McDonnell*, 1990], LI1 catchment at Llyn Brianne, Wales [*Soulsby*, 1992], Plastic Lake basin 1-08, Canada [*Peters et al.*, 1995], and Tatsunokuchi-yama Experimental Forest, Japan [*Tani*, 1997]. The water flow processes in headwater catchments can generally be described as follows: in humid, soil-mantled, and vegetated catchments, most of the rainwater infiltrates into and flows downward through the permeable soil layers, eventually reaching a less permeable layer and forming a transient perched groundwater table. The soil-bedrock interface has typically been assumed to form such a boundary between permeable and less permeable layers. Accordingly, water, driven by surface or bedrock topography, flows laterally along the boundary, sometimes via soil pipes, discharging into stream channels. Such conceptual models suggest that groundwater forms on the soil-bedrock interface in response to storm events and that subsurface flow through soil layers controls runoff generation in headwater catchments.

[3] Increasing knowledge of water flow processes in headwater catchments, as well as dramatic progress in computer processing capabilities and the establishment of geographic information systems (GISs), have contributed to a number of physically based models for simulating runoff generation [e.g., *Beven and Kirkby*, 1979; *O'Loughlin*, 1986; *Grayson et al.*, 1992; *Wigmosta and Burges*, 1997; *VanderKwaak and Loague*, 2001; *Downer and Ogden*, 2004] and shallow landslide occurrence [e.g., *Okimura and Ichikawa*, 1985; *Montgomery and Dietrich*, 1994; *Wu and Sidle*, 1995; *Rosso et al.*, 2006] in headwater catchments. Although these models have succeeded to some extent in simulating saturated areas or streamflow generation and in detecting areas prone to shallow landslides within the catchment, complete agreement between simulated and observed phenomena has, unfortunately, rarely been achieved. Such disagreement has generally been attributed to uncertainty in soil properties, such as thickness, hydraulic conductivity, and cohesion, which should be spatially variable but are often regarded as constant throughout the catchment because of limited data.

[4] Water flow processes other than those incorporated in these models can also produce discrepancies. While the

[1] Laboratory of Erosion Control, Department of Forest Science, Graduate School of Agriculture, Kyoto University, Kyoto, Japan.


0043-1397/08/2007WR006610

underlying bedrock can make important contributions to water flow, modeling studies have considered only surface conditions (i.e., topography and vegetation) and soil properties. Although subsurface flow through bedrock has conventionally been ignored in modeling small headwater catchments, many recent studies have suggested the contribution of bedrock groundwater flow to hydrological processes and landslides in headwater catchments. *Kosugi et al.* [2006] used pressure head measurements in shallow bedrock to demonstrate that unsaturated bedrock infiltration dominantly occurs in the middle-slope to upslope regions where a thick soil layer dampens rainfall intensity. The ratio of bedrock infiltration to annual precipitation in their small unchanneled catchment ranged from 35 to 55% [*Kosugi et al.*, 2006]. For small granitic catchments in central Japan, *Terajima et al.* [1993] estimated that the ratio exceeded 18.2%. Tracer experiments have further confirmed the existence of bedrock infiltration [e.g., *Wilson et al.*, 1993; *Noguchi et al.*, 1999; *Frazier et al.*, 2002; *Legout et al.*, 2007].

[5] Hydrometric [e.g., *Haria and Shand*, 2004] and hydrochemical [e.g., *Mulholland*, 1993; *Burns et al.*, 1998; *Katsuyama et al.*, 2005; *Soulsby et al.*, 2007] evidence has suggested that groundwater that has infiltrated into bedrock discharges slowly into soil layers and contributes to base flow. Runoff of bedrock groundwater often strongly influences the generation of saturated zones in soil layers. Studies have shown that bedrock groundwater exfiltrates into the overlying soil layers in areas adjacent to a stream channel [*McGlynn et al.*, 1999; *Uchida et al.*, 2003a; *Hattanji and Onda*, 2004]. *Uchida et al.* [2003b] provided quantitative information on this phenomenon in a granitic headwater catchment (0.10 ha) in central Japan; during base flow periods, bedrock groundwater, which contributed to 50 to 95% of the streamflow, seeped into overlying soil layers in a very small area accounting for 0.5 to 2.0% of the entire catchment near the channel head.

[6] Studies have also examined the contribution of subsurface flow through bedrock to soil mantle groundwater generation during storm events. *Wilson and Dietrich* [1987] suggested that bedrock groundwater exfiltrates into soil layers during rainfall events, strongly influencing the piezometric response of the overlying colluvium. Sprinkler and tracer experiments performed in a steep, unchanneled CB1 catchment underlain by sandstone revealed that saturated subsurface flow crosses back and forth between the near-surface bedrock and overlying colluvium, leading to the development of a patchily distributed saturated zone in the colluvium [*Anderson et al.*, 1997; *Montgomery et al.*, 1997]. *Wilson and Dietrich* [1987] and *Montgomery et al.* [1997] remarked that such interaction between the colluvium and shallow bedrock is very likely to trigger landslides. *Montgomery et al.* [2002] documented that the occurrence of debris flow resulting from a landslide in a CB2 catchment coincided with the commencement of water discharge from the shallow bedrock into overlying colluvium in the neighboring CB1 catchment. Field observations of landslide-induced debris flow scarps [*Everett*, 1979] and differences in the lag time between the peak rainfall intensity and peak runoff rate among small catchments with different geology [*Onda et al.*, 1999] have also implied the contribution of bedrock groundwater to landslide events.

[7] Although these previous studies have suggested the importance of bedrock groundwater to soil mantle groundwater generation and shallow landslides, such suggestions have typically been based on observations of the soil mantle and streamflow conditions or piezometric and tensiometric measurements within shallow bedrock. Such evidence can be obtained relatively easily and can indeed offer credible explanations for the observed phenomena and imply the contribution of bedrock; however, it is difficult to verify these inferences because of the lack of quantitative and qualitative information regarding conditions within the entire bedrock. To better understand the effects of bedrock that give rise to these phenomena, direct measurements of the bedrock groundwater level, chemistry, and temperature are needed.

[8] In this study, we observed soil mantle groundwater dynamics in a steep headwater catchment in central Japan (Nishi'otafuku-Yama Experimental Watershed). *Kosugi et al.* [2008] reported that soil mantle groundwater in a single well in this watershed showed two completely different responses. One response involved ephemeral-type groundwater (referred to as "EG" in this study), which was generated only during rainfall events and disappeared rapidly after the events ceased. The other response involved semiperennial-type groundwater ("SPG"), which remained formed for more than several months. A physically based surface-hydrological model that reproduced the dynamics of EG very well failed to describe the behavior of SPG [*Kosugi et al.*, 2002]. *Kosugi et al.* [2008] revealed that the sources of EG were storm rainwater and pre-event solum water, whereas the source of SPG was deep bedrock groundwater; they also noted the importance of clarifying how these two types of groundwater (i.e., EG and SPG) are synthesized at each point in the catchment for better understanding of the effects of bedrock groundwater on surface hydrological processes and for accurate prediction of the timing, location, and scale of landslides.

[9] The present study involved the long-term observations of soil mantle groundwater dynamics at four points in the Nishi'otafuku-Yama Experimental Watershed as well as direct monitoring of bedrock groundwater dynamics using deep boreholes. By combining hydrometric, hydrochemical, and thermal data, we clarify how deep bedrock groundwater affected the soil mantle groundwater at each point and discuss water flow processes in the catchment.

## 2. Methods

### 2.1. Study Site

[10] The Nishi'otafuku-Yama Experimental Watershed (34°46′N, 135°16′E) is located in Hyogo Prefecture, central Japan (Figure 1). The catchment, covering 1.87 ha, is located near the summit of Mt. Rokko (932 m), and covered with a closed secondary forest with dense undergrowth of bamboo grasses. Elevation in the catchment ranges from 740 to 875 m above sea level, the mean gradient is 35°, and the mean annual precipitation is approximately 1800 mm. The catchment is unchanneled, except at its outlet, where a stream flows almost perennially from a spring (located between point D and the weir; Figure 1c).

[11] The whole catchment is underlain by granitic bedrock called Rokko granite. The soil depth to the bedrock

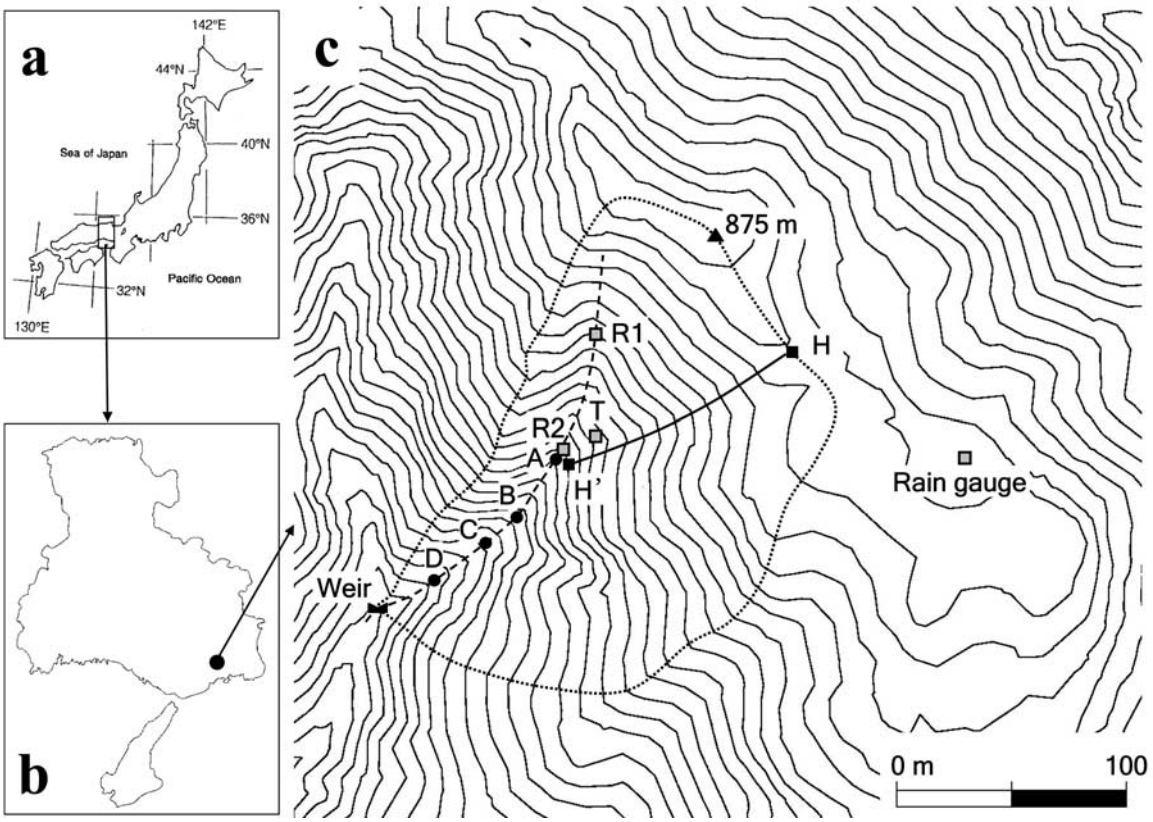


**Figure 1.** Maps of (a) Japan, (b) Hyogo Prefecture, and (c) the Nishi'otafuku-Yama Experimental Watershed. Map (Figure 1c) has a contour interval of 5 m.

surface ranges from 25 to 270 cm, and it is greater in the main hollow and the middle part of the west-facing slope. The saturated hydraulic conductivity, $K_s$, of the soils, measured for 30 undisturbed samples collected 0–50 cm deep at six points (on the H-H' line; Figure 1c), ranged from $1.2 \times 10^{-2}$ to $2.1 \times 10^{-1}$ cm $s^{-1}$ [*Hendrayanto et al.*, 1999].

[12] We observed evidences of old shallow landslides around points R1 and B, and colluvium including gravel along the main hollow from point A to the weir (Figure 1c). The colluvium was 92 cm thick near point B. Here, the $K_s$ values measured using undisturbed soil core samples 100 mL in volume (n = 3) were $1.0 \times 10^{-1} - 1.2 \times 10^{-1}$ cm $s^{-1}$ and $1.4 \times 10^{-1} - 2.8 \times 10^{-1}$ cm $s^{-1}$ at depths of 10 and 30cm, respectively. Below 54 cm, the soil mantle contained many gravels reaching approximately 30 cm in diameter. Three 100-mL soil core samples collected between the gravels had $K_s$ values ranging from $1.1 \times 10^{-1}$ to $1.9 \times 10^{-1}$ cm $s^{-1}$ [*Kosugi et al.*, 2008]. For more information on the experimental watershed, see *Kosugi et al.* [2008].

### 2.2. Observations

[13] Observation wells were manually excavated to the bedrock surface at four points (A, B, C, and D; Figure 1c) in June 2004. These wells were constructed using PVC pipes 5.5 cm in inner diameter perforated with 5-mm-diameter holes throughout the subsurface, the total area of which was equivalent to 9% of the total lateral area of the pipe (Figure 2). The depths of wells A–D (equivalent to the soil depth at each point) were 227, 115, 130, and 140 cm, respectively. We installed a water level gauge (MC-1100W, STS Sensor Tecknik Sirnach AG, Sirnach, Switzerland) at the bottom of each observation well (Figure 2) and monitored the groundwater level and temperature in the wells simultaneously at 5-min intervals. When groundwater formed in the well, the temperature in the well represented that of the groundwater; otherwise it represented that of soil at the bottom of the well. Precipitation was measured at 10-min intervals using a tipping bucket rain gauge placed at a clearing approximately 50 m from the catchment boundary near the ridge (Figure 1c). We commenced these observations in June 2004.

[14] We also measured the soil temperature profile at a point (T in Figure 1c) at 5-min intervals using thermocouples from 3 September 2004 to 18 May 2005 and a thermistor-type temperature probe (Model 107 Temperature Probe, Campbell Scientific, Logan, UT, USA) after that period. Measurement depths were 10, 30, 60, 100, and 200 cm from the ground surface.

[15] In August 2005, boreholes were drilled at points R1 and R2 in Figure 1c using a hydraulic-feed-type boring machine. The total depths of the boreholes were 35 and 38 m, respectively, and the borehole diameter was 6.6 cm. Core samples obtained from the boreholes indicated that a soil layer and highly ($D_L$ to $C_L$ classes) and moderately ($C_L$ to $C_M$ classes) weathered bedrock layers occurred at 0.0–1.8, 1.8–27.0, and 27.0–35.0 m depths in borehole R1 and 0.0–1.6, 1.6–19.3, and 19.3–33.5 m depths in R2. For 33.5–38.0 m depths in R2, a weakly weathered ($C_M$ class) bedrock layer was observed. The $K_s$ value of the bedrock

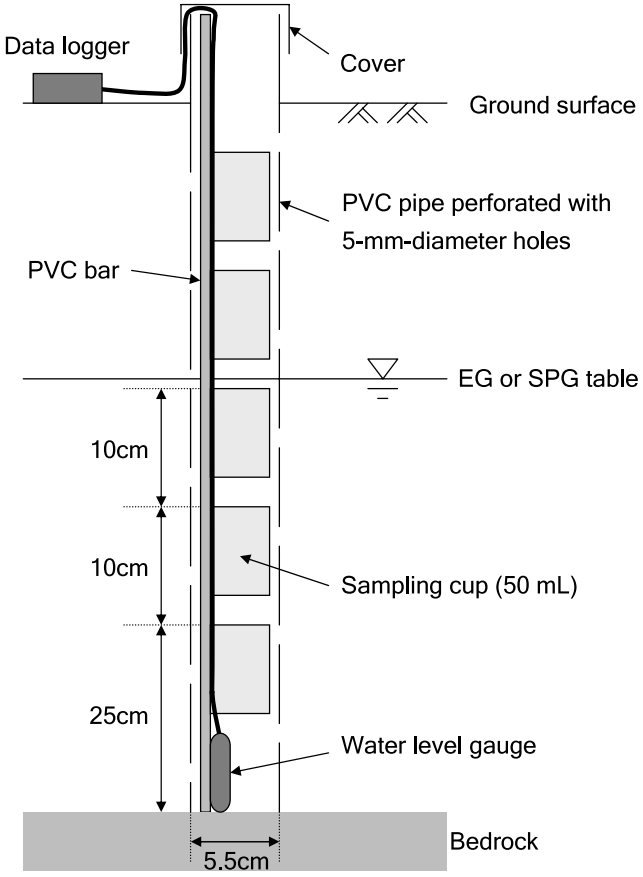


**Figure 2.** Schematic diagram of a device used for soil mantle groundwater sampling in wells A–D.

core samples, measured in the laboratory using the method of *Katsura et al.* [2006], was $8.9 \times 10^{-5}$ (at depth of 3.93 m in borehole R1) and $2.9 \times 10^{-4}$ cm $s^{-1}$ (2.63 m in R2) for the highly weathered layer; $3.4 \times 10^{-4}$ (27.06 m in R1) and $2.1 \times 10^{-6}$ cm $s^{-1}$ (21.73 m in R2) for the moderately weathered layer; and $2.2 \times 10^{-9}$ cm $s^{-1}$ (36.80 m in R2) for the weakly weathered layer.

[16] To sustain the boreholes, PVC pipes, the bottom 8 and 16 m of which were perforated with four 5-mm-diameter holes per 5 cm, were inserted into boreholes R1 and R2, respectively. On 29 September 2005, we began monitoring the bedrock groundwater level in the boreholes and the temperature at the bottom of the boreholes at 5-min intervals using the same water level gauge mentioned above.

[17] For silica ($SiO_2$) concentration analyses, we collected groundwater and rainwater samples approximately once a month. To collect soil mantle groundwater samples, we kept a PVC bar, with 50-mL polyethylene cups attached at 10-cm intervals from 25 cm above the bottom through the ground surface, in each observation well A–D (Figure 2); groundwater samples were collected individually from each cup at monthly samplings. Because each cup trapped groundwater when the groundwater level rose above the top of the cup, the water collected from each cup represented the groundwater at the level last recorded at the depth of the corresponding cup before the sampling [*Kosugi et al.*, 2008]. Coupling this method with the groundwater level measurement in each well allowed us to characterize the dynamics of the groundwater $SiO_2$ concentration. Groundwater in boreholes R1 and R2 was manually drawn using a rope with sampling cups attached. Rainwater was collected in a bottle with a 24-cm-diameter funnel, located near the tipping bucket, from which samples were taken. All water samples collected were sealed in 50-mL polyethylene bottles, and $SiO_2$ concentration was measured by the molybdenum yellow method in the laboratory [*Yokoyama et al.*, 1993].

[18] On 18 February 2007, resistivity image profiling was carried out using a pole-pole electrode array [*Shima et al.*, 1995]. To explore depths within 50 m of the ground surface, 93 electrodes were installed at 2-m intervals over a length of 184 m along the main hollow (dashed line in Figure 1c). An inverse analysis based on the finite element method for solving a two-dimensional electric potential distribution was applied to correct the observed apparent resistivity pseudosection [*Shima et al.*, 1995].

## 3. Results

### 3.1. Groundwater Level

#### 3.1.1. Soil Mantle Wells A–D

[19] Figure 3 shows the daily rainfall and groundwater level dynamics in each observation well and borehole. Figure 3a includes the variation in the antecedent precipitation index with the half-life of $M$ hours, $P_M(t)$ [mm], calculated as

$$P_M(t) = P_M(t-1)\exp(\ln 0.5/M) + R_h(t)\exp(\ln 0.5/2M) \quad (1)$$

where $t$ [h] is the time and $R_h(t)$ [mm] is the total precipitation from $t-1$ to $t$ [*Suzuki and Kobashi*, 1981]. We used 1752 h (= 73 d) for the value of $M$ (i.e., $P_{73d}$) because $P_{73d}$ has been shown to be a good index for evaluating the long-term effect of antecedent rainfall [*Kosugi et al.*, 2008].

[20] Whereas a moderate amount of rainfall was recorded in 2004 (1712.2 mm) and 2006 (1883.8 mm), the annual rainfall in 2005 was extremely small (1149.4 mm) compared to the average value (approximately 1800 mm). This is reflected in the variation in $P_{73d}$ (Figure 3a); while $P_{73d}$ was always greater than 432.8 mm throughout the observation period in 2004, $P_{73d}$ was less than 432.8 mm for 84.8% of the entire period in 2005. $P_{73d}$ eventually decreased to 236.0 mm on 31 January 2006 but then began to increase as the catchment received more rainfall, especially in May 2006. Afterward, $P_{73d}$ was always greater than 424.3 mm until the end of 2006.

[21] At point A (Figure 3b), groundwater developed in response to rainfall events and always disappeared rapidly after the events ceased. The response of groundwater generation showed good correspondence to variation in daily rainfall rather than in $P_{73d}$. This type of groundwater in soil layers has been widely observed in various steep headwater catchments [e.g., *Bazemore et al.*, 1994; *Tsuboyama et al.*, 2000]. We refer to this ephemeral-type groundwater as EG in this study. The maximum EG level at point A during the observation period was −52.6 cm (i.e., 52.6 cm below the ground surface), observed on 11 May 2006.

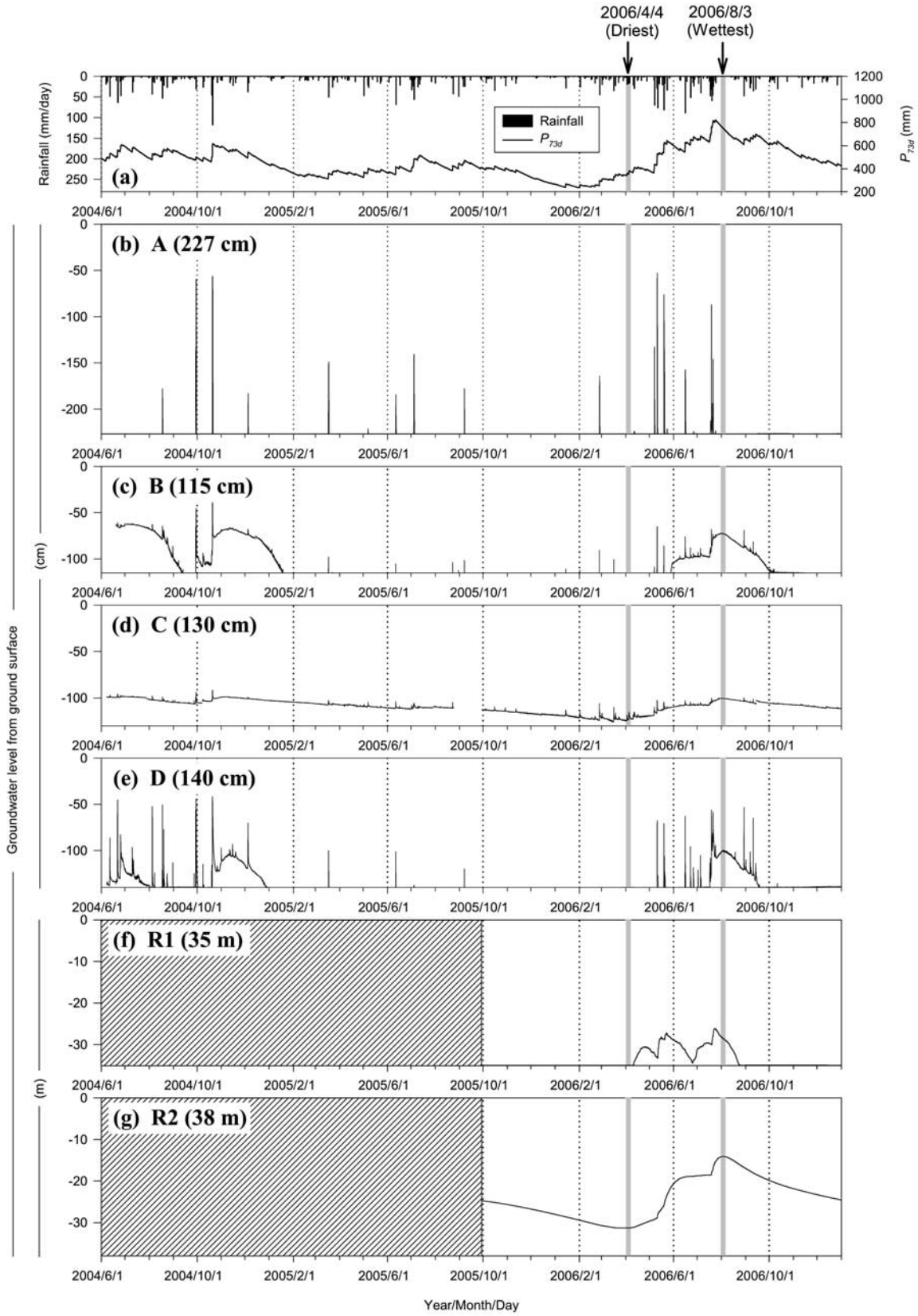


**Figure 3.** (a) Daily rainfall with $P_{73d}$, and the groundwater level observed in (b–e) wells A–D and (f, g) boreholes R1 and R2.

[22] At point B (Figure 3c), groundwater had already formed at the beginning of the observations (19 June 2004). This groundwater remained formed for about three months until 11 September 2004. It was very anomalous for the groundwater in soil layers to show such dynamics in steep headwater catchments. We refer to this semiperennial-type groundwater as SPG in this study. Note that EG components could also occur in response to rainfall during periods of SPG generation; for example, the 3–5 August 2004 event with a total rainfall of 56.2 mm ephemerally increased the groundwater level by 6.0 cm from the SPG level of −68.6 cm that had already developed before the event.

[23] SPG generation was noted three times at point B during the observation period. The first SPG had, as described above, already developed at the beginning of the observation. The second SPG was generated on 29 September 2004, when a rainfall event triggered the development of EG (the maximum level was −45.1 cm) and the following SPG. The total rainfall of this event was 31.8 mm, the 42nd largest of the 199 rainfall events during the observation period. While such a medium-sized rainfall event did generate SPG, the second largest event (6–11 May 2006, total rainfall: 186.8 mm) produced EG without SPG. The third occurrence of SPG was on 28 May 2006, when no rainfall was observed. The generation of this SPG event is probably attributable to the large amount of rainfall delivered to the catchment in the previous days in May 2006, as indicated by the steep increase in $P_{73d}$ (Figure 3a). Comparison with the variation in $P_{73d}$ (Figure 3a) demonstrates that these three periods of SPG generation exhibited relatively good correspondence to the periods in which $P_{73d}$ exceeded approximately 500 mm. The SPG dynamics at point B thus suggest that SPG generation can be explained not by the scale of individual rainfall events, but rather by the long-term effects of antecedent rainfall [*Kosugi et al.*, 2008].

[24] The SPG had already developed at the beginning of the observations (7 June 2004) at point C (Figure 3d) and remained formed until the end of the observations. The waveform of the SPG level dynamics at point C was very similar to the variation in $P_{73d}$ (Figure 3a), again suggesting a long-term effect of antecedent rainfall on SPG dynamics. Even rainfall events causing a significant rise in the groundwater level at point A raised the groundwater level at point C only slightly. The maximum and minimum groundwater levels throughout the observation period were −91.5 and −126.1 cm, respectively, emphasizing the very small range of variation in groundwater levels at point C. It should be noted that SPG gradually decreased, but never disappeared in spite of the very small amount of rainfall in 2005.

[25] At point D (Figure 3e), SPG was observed three times during the observation period: from 7 June through 2 August 2004, 19 October through 29 December 2004, and 17 July through 18 September 2006. These three periods of SPG generation corresponded relatively well to periods when $P_{73d}$ was greater than approximately 600 mm (Figure 3a). Soil mantle groundwater at point D was characterized by a larger EG level increase than that at points B and C in response to rainfall during periods of SPG generation. For example, the rainfall event on 4–5 December 2004 (total rainfall: 54.0 mm), which occurred when SPG had already formed at points B, C, and D, ephemerally increased the groundwater level by 5.8, 1.5, and 48.2 cm, respectively.

[26] While EG always exhibited flashy peak in response to rainfall, SPG generally had a broad peak. Fairly synchronous SPG peaks were observed three times at points B (Figure 3c), C (Figure 3d), and D (Figure 3e). The first peaks cannot be discussed in detail here because they were observed immediately after commencement of the observations. The second peaks were observed on 10 November 2004 for point B and 9 November 2004 for points C and D. The third peaks were observed on 1 August, 31 July, and 3 August 2006 for points B, C, and D, respectively. Rain gauge records indicate that the catchment received less than 1 mm of rainfall on each of these dates, suggesting that SPG level dynamics were not controlled by individual rainfall events. Instead, SPG levels seemed to peak 12–21 d after the peak of preceding large rainfall events; the second and third SPG peaks were probably produced by the preceding large rainfall events peaking on 20 October 2004 (total rainfall: 170.8 mm) and 19 July 2006 (total rainfall: 222.0 mm), respectively. These SPG peak analyses, together with the good correspondence between the SPG waveforms and the variation in $P_{73d}$, suggest that effects of antecedent rainfall were reflected in SPG dynamics in wells B, C, and D. A long time lag was evident in these cases.

#### 3.1.2. Boreholes R1 and R2

[27] In borehole R1 (Figure 3f), the groundwater level within the bedrock was observed only on 10 April through 25 August 2006. Although the borehole depth was as deep as 35 m, the groundwater level showed relatively rapid response to rainfall events. The maximum groundwater level throughout the observation period was −26.1 m on 24 July 2006; it was probably created by the large rainfall event peaking 4 d earlier (15–21 July 2006, total rainfall: 222.0 mm).

[28] In borehole R2 (Figure 3g), the groundwater level within the bedrock was observed at the beginning (i.e., 29 September 2005) through the end of the observation. The groundwater response to rainfall was milder than that in borehole R1. The maximal R2 groundwater level (−14.1 m) was observed on 3 August 2006, 14 d after the peak of the large rainfall event on 15–21 July 2006.

#### 3.1.3. Relationship Between the Soil Mantle and Bedrock Groundwater Level Dynamics

[29] Comparison of groundwater level dynamics (Figure 3) demonstrates that the waveforms of SPG observed at points B, C, and D were very similar to the waveform of the bedrock groundwater level in borehole R2. Figure 4 shows the relationships between the groundwater level in each soil mantle well (A-D) and in borehole R2 observed from 29 September 2005 through the end of the observations. The plots were classified into three groups according to the style of soil mantle groundwater generation: (1) EG generated in the periods of no SPG generation (labeled "EG alone" in Figure 4, red open circles), (2) EG generated in the periods of SPG generation ("EG with SPG," pink open circles), and (3) SPG ("SPG," blue open circles).

[30] The EG-alone-type groundwater at point A and the EG-with-SPG-type groundwater at point C were generated regardless of the groundwater level in borehole R2. The level of these types of groundwater often rose and dropped

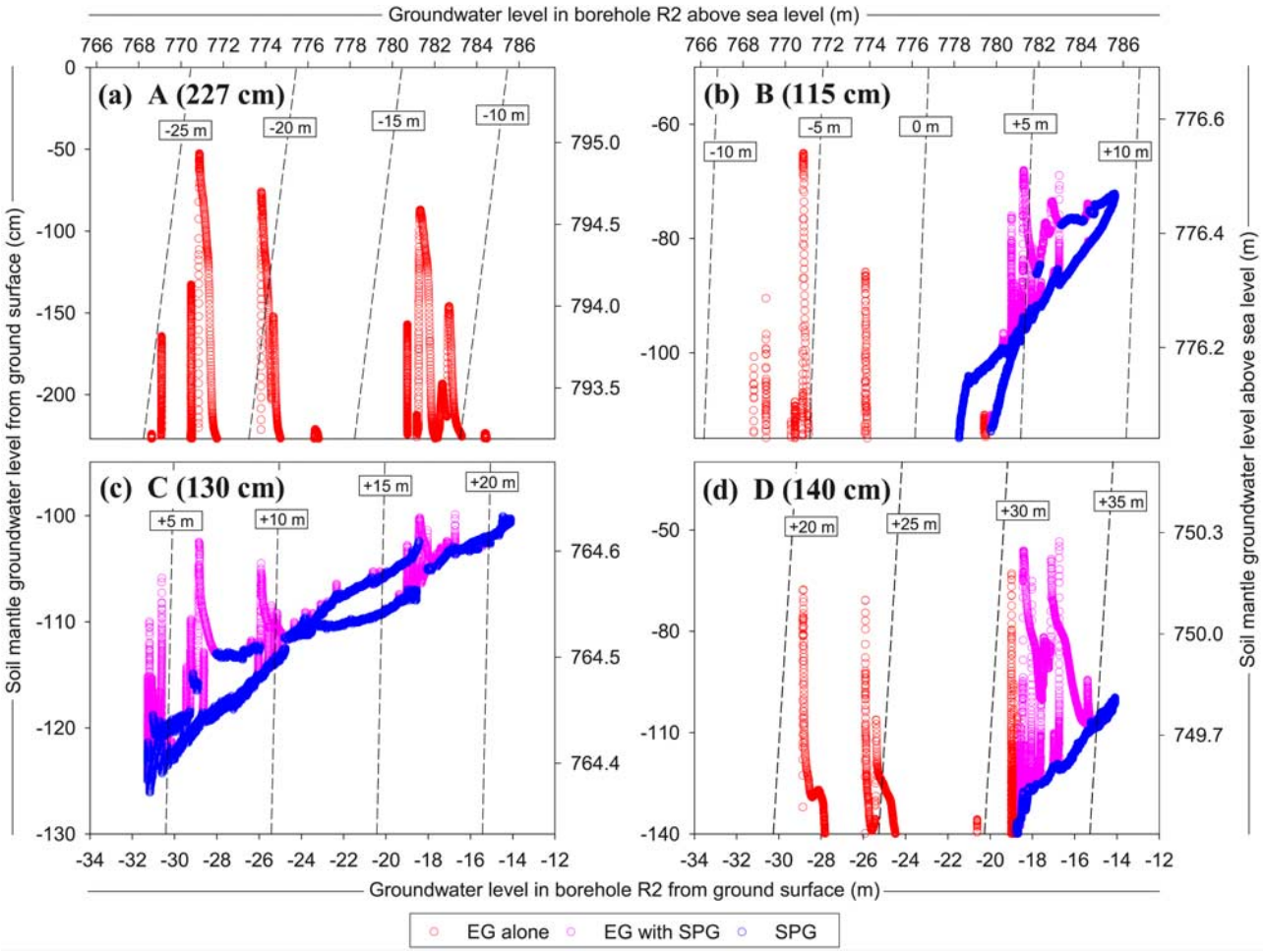


**Figure 4.** Relationships between the groundwater level in the soil mantle wells A–D (the ordinate) and in borehole R2 (the abscissa). The elevation corresponding to the groundwater level is also shown. Dashed lines represent the contour lines of the relative height of the abscissa to the ordinate; this value is shown in the open rectangles.

in spite of the decrease and increase in the R2 level, respectively. The SPG level at points B, C, and D, on the other hand, exhibited a strong positive correlation with the bedrock groundwater level in borehole R2 although the increase ratio of the SPG level to the R2 level was very low. SPG never occurred at points B and D when the bedrock groundwater table in borehole R2 was lower than −21.5 m and −18.8 m, respectively. Moreover, the SPG peaks observed at points B, C, and D almost coincided with the maximal bedrock groundwater level in borehole R2. These findings clearly demonstrate that there was no connection between EG (both EG-alone-type and EG-with-SPG-type) and groundwater level dynamics within the bedrock; however, a close connection was evident for SPG.

[31] Using the measured groundwater levels and their corresponding elevation values, Figure 5 shows the longitudinal section of the catchment including the groundwater table observed on 4 April and 3 August 2006, when no rainfall was observed. On 4 April 2006, the catchment was assumed to have been under its driest condition because SPG had not developed at points B and D, and the bedrock groundwater level in borehole R2 was minimal (Figure 3). On 3 August 2006, on the other hand, SPG had developed at points B, C, and D, and the groundwater levels in these wells and borehole R2 approached maximal levels in 2006 (Figure 3), indicating the wettest catchment conditions during the study period. The estimated groundwater tables crossed the soil-bedrock interface at an elevation of approximately 768 m between points B (777 m) and C (766 m) on 4 April 2006, and at approximately 780 m between points A (795 m) and B (777 m) on 3 August 2006 (Figure 5), which consistently explained the absence and generation of SPG observed at point B on each date and the close connection of SPG to bedrock groundwater level dynamics. These hydrometric observations suggest that water coming from deep bedrock layers formed SPG in soil layers and that bedrock groundwater level dynamics determined the location, timing, and level of SPG generation.

### 3.2. $SiO_2$ Concentrations

[32] Groundwater chemistry provides evidence for determining the sources of soil mantle groundwater. Figure 6 shows groundwater levels and $SiO_2$ concentrations observed in wells A–D and boreholes R1 and R2. The concentration is indicated by open circles, and a larger circle denotes a higher concentration value.

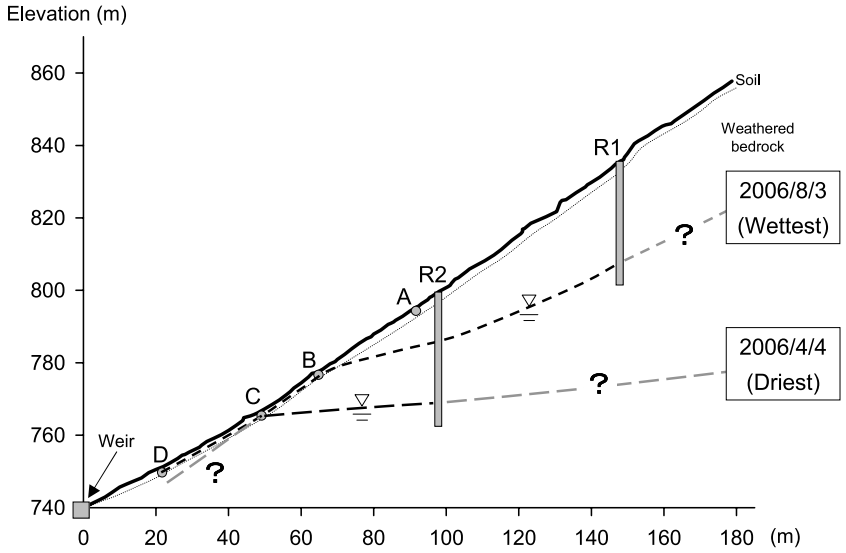


**Figure 5.** Longitudinal section of the study site showing the groundwater tables observed on 4 April and 3 August 2006.

[33] At point A (Figure 6b), where only EG-alone-type groundwater was observed, all groundwater samples had very low $SiO_2$ concentrations, ranging from 0.07 to 0.19 mmol $L^{-1}$. The EG-alone-type groundwater that developed on 11 May 2006 at point B (Figure 6c) also exhibited very low $SiO_2$ concentrations (0.12–0.16 mmol $L^{-1}$). On the other hand, the $SiO_2$ concentrations of SPG observed at points B (Figure 6c), C (Figure 6d), and D (Figure 6e) were 0.32–0.36, 0.35–0.39, and 0.31–0.35 mmol $L^{-1}$, respectively; these values were 1.6 to 5.6 times higher than the $SiO_2$ concentrations of the EG-alone-type groundwater observed at points A and B. When rainfall events produced EG during periods of SPG generation (i.e., EG-with-SPG-type groundwater) at points B and C, the $SiO_2$ concentrations of such groundwater samples had low to high values between 0.11 and 0.44 mmol $L^{-1}$. For example, the EG-with-SPG-type groundwater that developed at point B from the large rainfall event on 19–23 October 2004 (total rainfall: 170.6 mm) exhibited low $SiO_2$ concentrations (0.11–0.14 mmol $L^{-1}$) like those of EG-alone-type groundwater; however the EG-with-SPG-type groundwater generated by the 29–30 August 2006 event (total rainfall: 51.0 mm) at the same point B exhibited high $SiO_2$ concentrations (0.29–0.31 mmol $L^{-1}$). At point D (Figure 6e), all EG samples (both EG-alone-type and EG-with-SPG-type) had relatively high $SiO_2$ concentrations of 0.22–0.34 mmol $L^{-1}$.

[34] Bedrock groundwater samples from borehole R1 (Figure 6f) had relatively high $SiO_2$ concentrations (0.24–0.28 mmol $L^{-1}$). The $SiO_2$ concentrations of samples from borehole R2 (Figure 6g) were always high (0.32–0.36 mmol $L^{-1}$) except for the sample collected on 25 July 2006 showing a slightly lower $SiO_2$ concentration of 0.24 mmol $L^{-1}$.

[35] Results of the $SiO_2$ concentration analyses are summarized in Figure 7. The EG-alone-type groundwater at points A and B exhibited very low $SiO_2$ concentrations ranging from 0.07 to 0.19 mmol $L^{-1}$. On the other hand, the $SiO_2$ concentrations of SPG at points B, C, and D were very high with a narrower range (0.31 to 0.39 mmol $L^{-1}$) than those of the EG-alone-type groundwater, and the concentration values were nearly the same as or only a little higher than those of bedrock groundwater samples from boreholes R1 (0.24–0.28 mmol $L^{-1}$) and R2 (0.24–0.36 mmol $L^{-1}$). These hydrochemical data clearly indicate that the source of SPG was deep bedrock groundwater. The EG-alone-type groundwater, with very low $SiO_2$ concentrations, probably consisted of water flowing only through soil layers because $SiO_2$ is contained little in rainwater and is mainly released as solutes to subsurface water through chemical weathering processes, and the greater silica availability with increasing depth causes the subsurface water $SiO_2$ concentration to increase with depth [*Scanlon et al.*, 2001]. Many previous studies conducted in granitic headwater catchments have consistently demonstrated that shallow or soil water has considerably lower $SiO_2$ concentrations than deep or bedrock groundwater [e.g., *Shimada et al.*, 1992; *Asano et al.*, 2003; *Uchida et al.*, 2003b; *Katsuyama et al.*, 2005]. The $SiO_2$ concentration of the EG-with-SPG-type groundwater at points B and D ranged between that of EG-alone-type groundwater and SPG at each point, suggesting that mixing of soil water (i.e., EG-alone-type groundwater) with bedrock groundwater (i.e., SPG) occurred at these two points when rainfall events ephemerally increased the groundwater level above the existing SPG level (i.e., EG-with-SPG-type groundwater).

### 3.3. Temperature

#### 3.3.1. Soil Temperature at Point T

[36] The daily average soil temperatures measured at point T are shown in Figure 8. The temperature exhibited sinusoidal seasonal variation at all measurement depths, and the amplitude and phase were damped and delayed, respectively, as the depth increased from 10 to 200 cm below the ground surface. The range of the temperature variation at −200 cm (Figure 8e) during the observation period was 6.9 to 16.1°C, emphasizing the damped seasonal temperature variation.

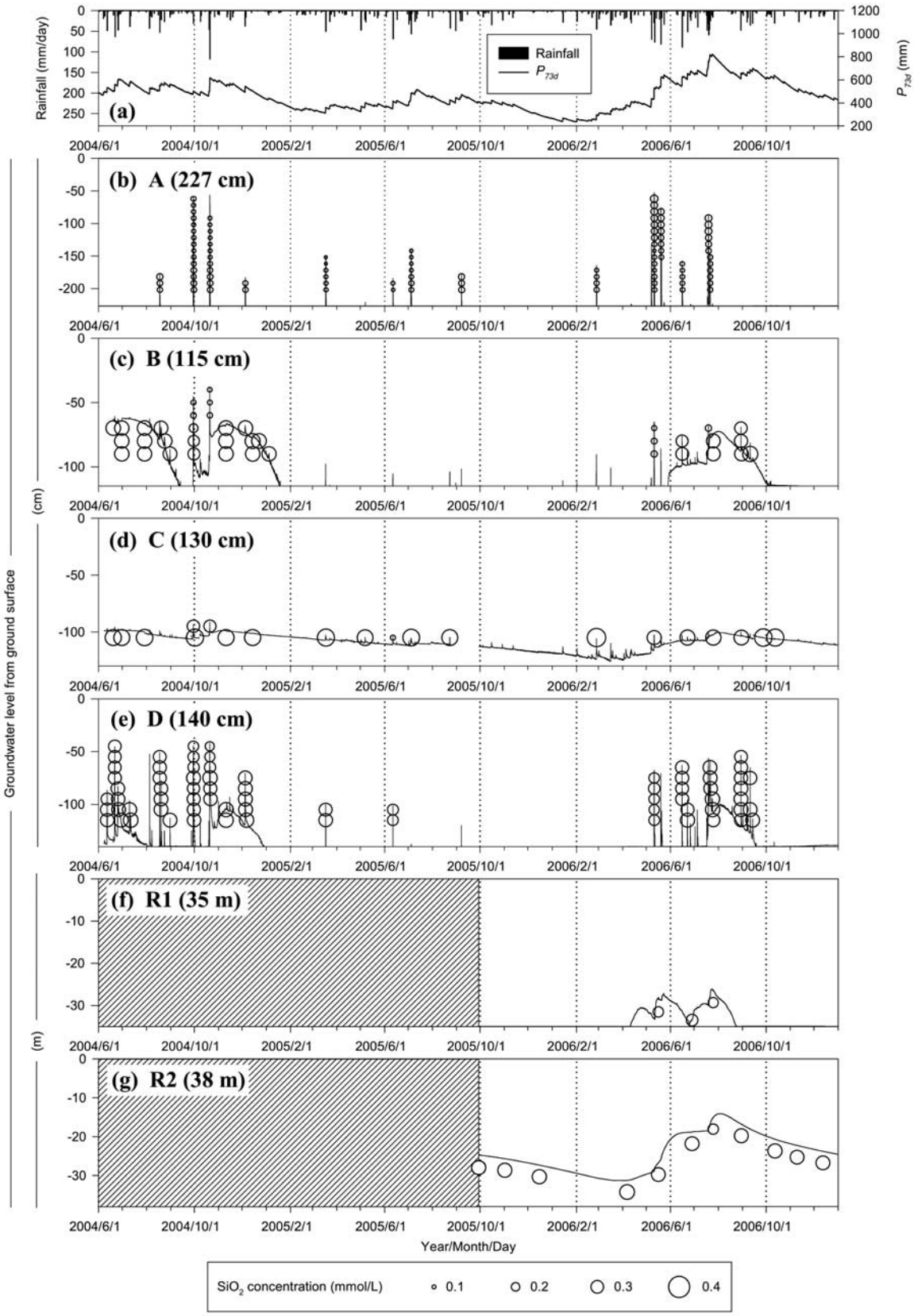


**Figure 6.** (a) Daily rainfall with $P_{73d}$, and the groundwater level along with $SiO_2$ concentrations observed in (b–e) wells A–D and (f, g) boreholes R1 and R2.

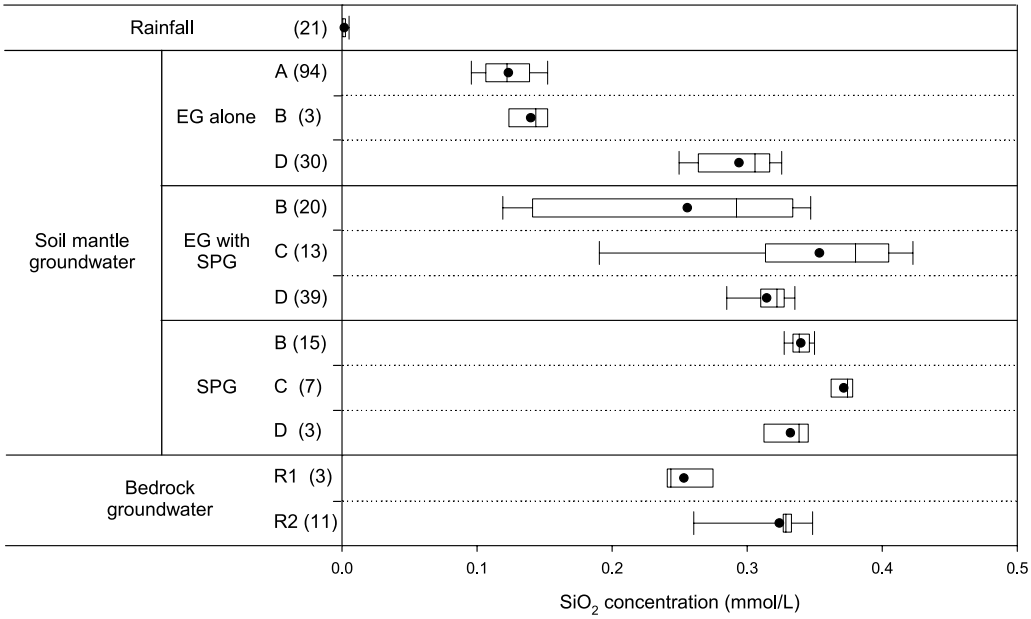


**Figure 7.** $SiO_2$ concentrations of rainfall and groundwater. Solid circles indicate the mean values. The sides of the box closest to and farthest from zero indicate the 25th and 75th percentiles, respectively, and the line within the box denotes the median. The lines to the left and right of the box represent the 10th and 90th percentiles, respectively. The number of the samples analyzed is given in parentheses.

### 3.3.2. Temperature in Soil Mantle Wells A–D

[37] Figure 9 shows the groundwater level and daily average temperature in wells A–D and boreholes R1 and R2. In Figures 9b–9e, two types of lines represent the temperature variation in the soil mantle wells: red lines for periods lacking SPG generation and blue lines for periods with SPG generation.

[38] At point A (Figure 9b), SPG was never generated during the observation period. Although some large rainfall events created EG, and the temperature in the well correspondingly increased in summer and decreased in winter, the temperature in the well showed sinusoidal seasonal variation with the highest and lowest values being 15.3 and 7.1°C, respectively.

[39] At point B (Figure 9c), the temperature in the well remained relatively constant (11.2–12.5°C) during the period of the first SPG generation (i.e., 19 July through 11 September 2004). Although the temperature suddenly began to rise after disappearance of the first SPG observed, the temperature in the well sharply dropped on 29 September 2004, when the medium-sized rainfall event led to the second SPG observed. After remaining relatively constant until the disappearance of this second SPG, the temperature suddenly dropped further and subsequently came to show sinusoidal seasonal variation until the generation of the third SPG on 28 May 2006. While the temperature during the second SPG period varied only slightly between 10.5 and 13.1°C, the temperature during the same period in the following year with no SPG generation (i.e., 29 September 2005 through 17 January 2006) varied from 5.1 to 17.6°C, suggesting damped temperature variation during the second SPG period. The temperature range during the third SPG period was 10.8 to 12.3°C, similar to that of the first and second SPG periods. Again, SPG generation strongly damped the temperature variation compared with the same period in the previous year with no SPG (i.e., 28 May through 2 October 2005), during which the temperature rose to 18.4°C. Thus, switching of the mode of the temperature variation, controlled by the generation and disappearance of SPG, was observed very clearly at point B.

[40] At point C (Figure 9d), where SPG occurred throughout the observation period, the temperature in the well varied sinusoidally between 9.2 and 13.0°C, suggesting a very narrow range of seasonal SPG temperature variation. Note that this temperature range was similar to that of well B during SPG periods.

[41] At point D (Figure 9e), whereas the temperature varied only slightly between 10.6 and 13.2°C during the three periods of SPG generation (i.e., 7 June through 2 August 2004, 19 October through 29 December 2004, and 17 July through 18 September 2006), the temperature exhibited sinusoidal seasonal variation during periods without SPG events. The damping effect of SPG on temperature in well D was observed most clearly during the third SPG period (i.e., 17 July through 18 September 2006); temperature was maximal (15.5°C) on 16 September in the previous year, which lacked SPG generation, but temperature in the third SPG period remained fairly constant between 12.4 and 12.9°C. It should be noted that the range of sinusoidal temperature variation in the absence of SPG was greater during the period from June 2005 through May 2006 (6.4–15.5°C) than during the period from June 2004 through May 2005 (8.6–14.0°C), although no clear difference was recognized in the range of the soil temperature variation between these two periods at all depths at point T (Figure 8).

[42] In summary, the temperature variation in soil mantle wells A–D (Figures 9b–9e) can be classified into two

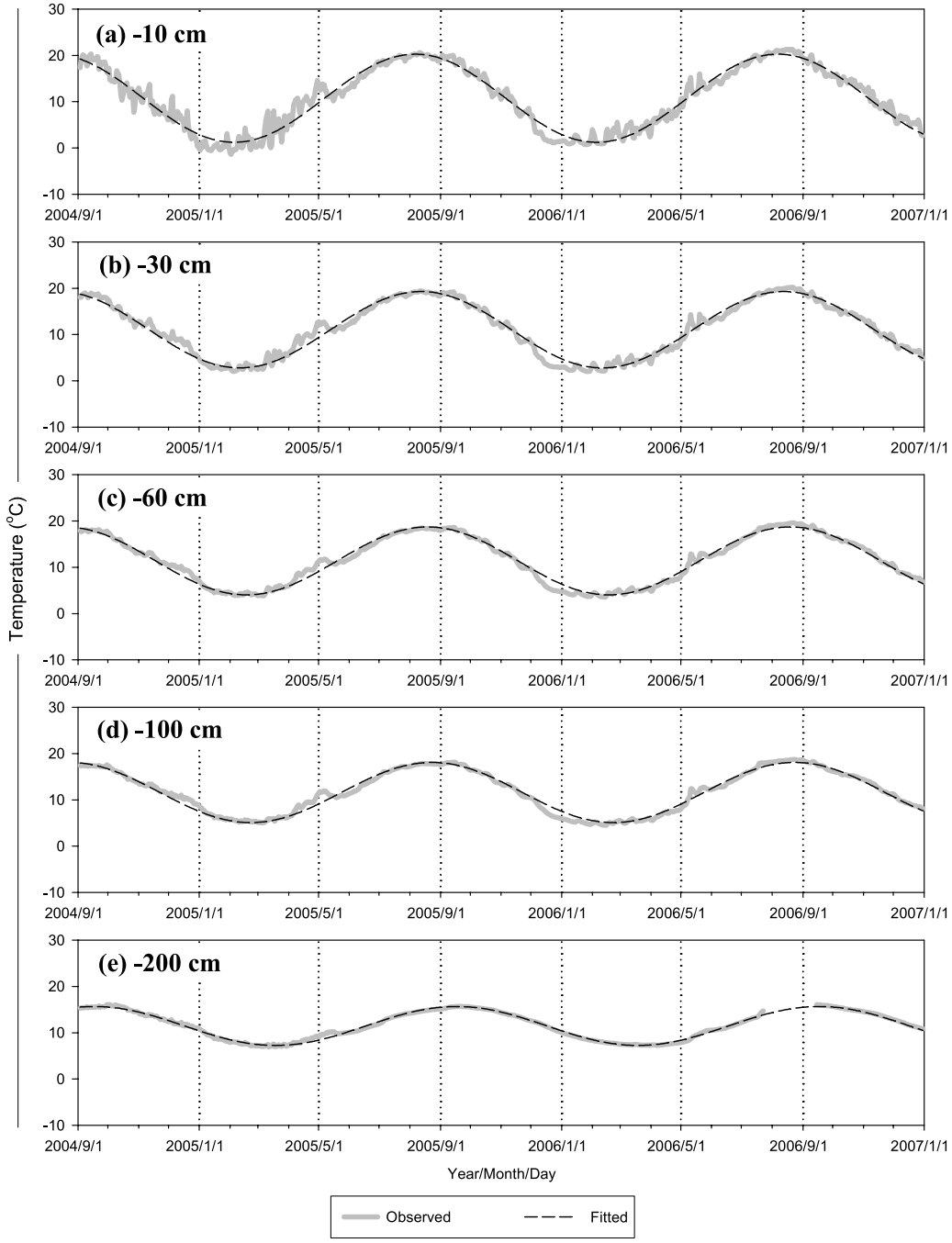


**Figure 8.** Daily average soil temperature measured at point T. The sinusoidal curve fitted to the observed temperature is also shown.

different modes. The first was characterized by relatively constant temperature (9.2–13.2°C); this mode occurred during SPG periods. The second was characterized by sinusoidal seasonal variation with large amplitude. This mode occurred in the absence of SPG events.

### 3.3.3. Temperature in Boreholes R1 and R2

[43] Figure 9 also includes the groundwater level and daily average temperature in boreholes R1 and R2. In borehole R1 (Figure 9f), the temperature varied little throughout the observation period regardless of whether groundwater was or was not observed in the borehole. The fairly constant temperature was also observed in borehole R2 (Figure 9g), in which groundwater was observed throughout the period. The temperature variation observed in boreholes R1 and R2 ranged from 11.4 to 12.8°C and 11.5 to 12.8°C, respectively. The ranges indicate almost identical temperature values and stability in the two boreholes.

### 3.3.4. Application of Thermal Conduction Theory to Observed Temperature

#### 3.3.4.1. Point T

[44] The soil temperature at point T showed sinusoidal seasonal variation at all measurement depths with greater depths exhibiting smaller amplitudes (Figure 8). To examine

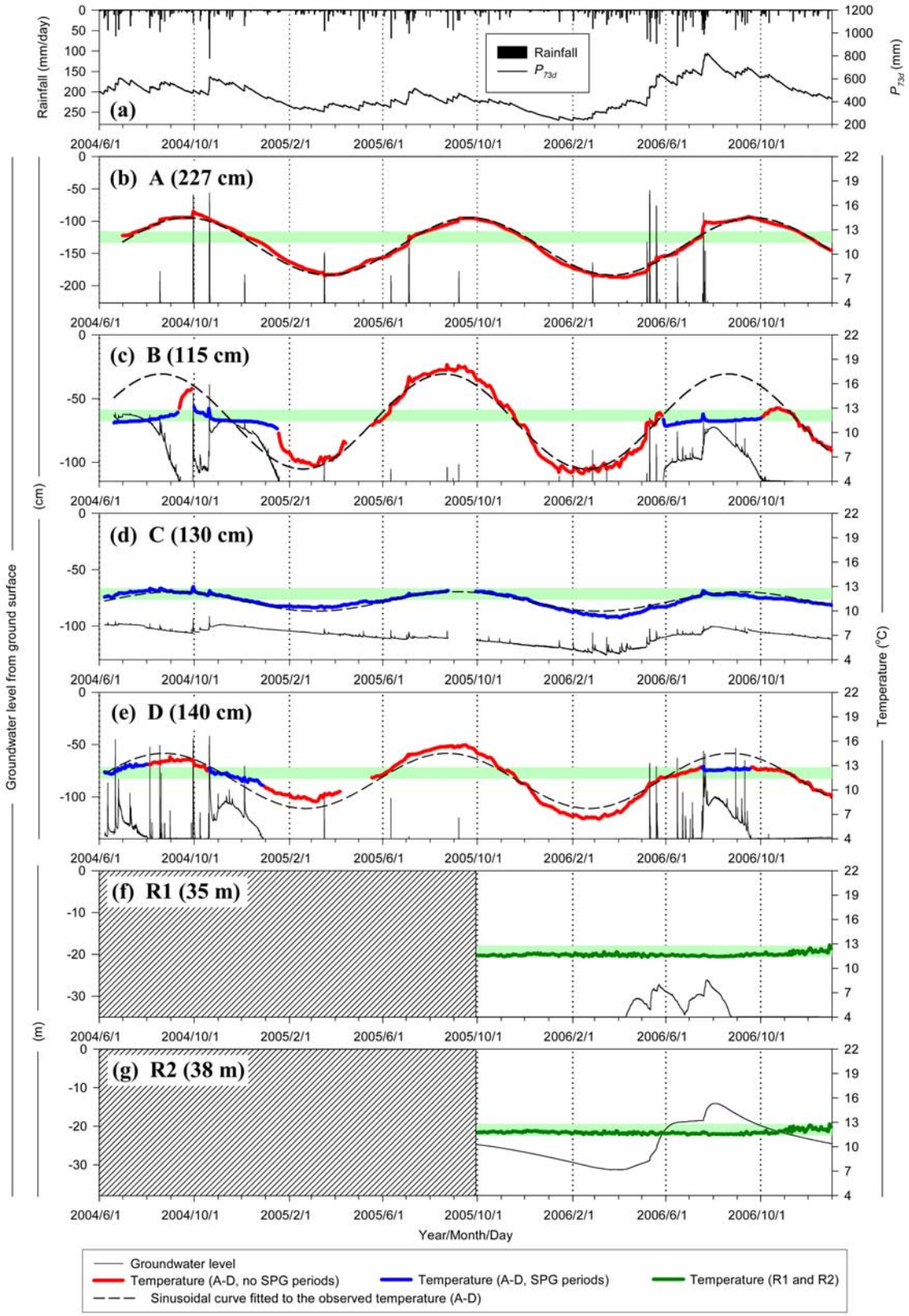


**Figure 9.** (a) Daily rainfall with $P_{73d}$, and the groundwater level and temperature observed at the bottom of (b–e) wells A–D and (f, g) boreholes R1 and R2. The dashed line indicates the sinusoidal curve fitted to the temperature observed during periods without SPG generation (wells A, B, and D; Figures 6b, 6c, and 6e) or with SPG generation (well C; Figure 6d). The light green line in Figures 6b–6g denotes the range of temperature variation observed in boreholes R1 and R2 (11.4–12.8°C).

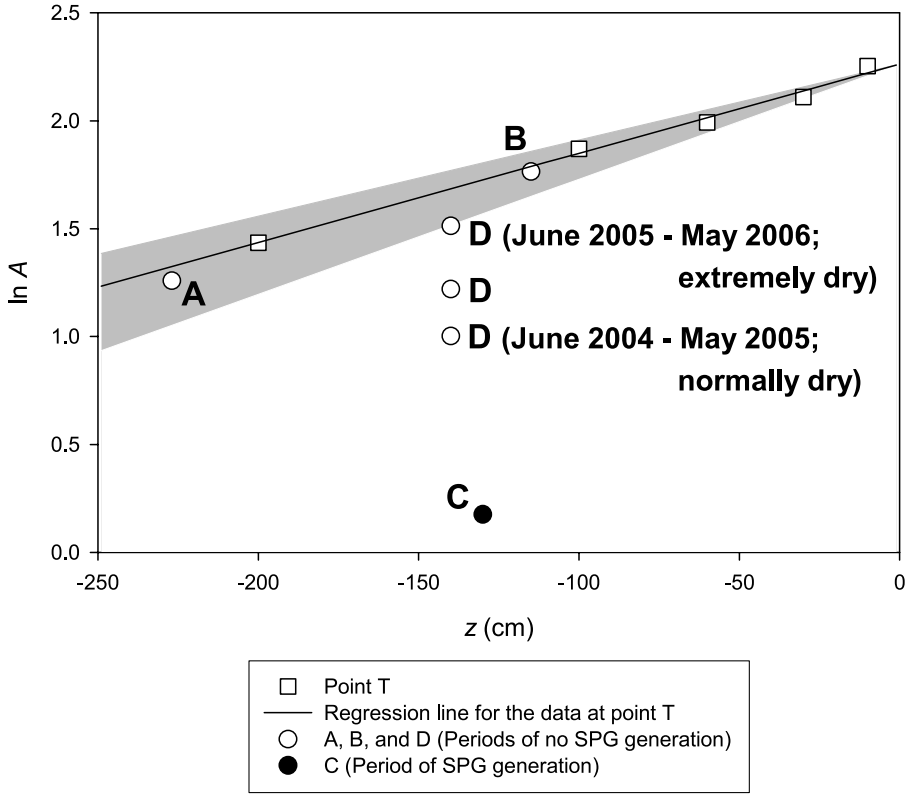


**Figure 10.** Relationship between ln $A$ and depth $z$. The $A$ values were calculated for the periods of no SPG generation (wells A, B, and D) or SPG generation (well C). The shaded area, estimated using the results of *Tani et al.* [1979] and *Uchida et al.* [2003b], indicates the range within which the data points were very likely to fall when groundwater advection did not affect soil temperature.

how the temperature variation in the soil layers at point T can be explained, a one-dimensional thermal conduction equation was employed. When heat transport by groundwater advection does not occur and thermal diffusivity of the soil is vertically homogeneous, the equation can be written as

$$\frac{\partial T(z,t)}{\partial t} = \kappa \frac{\partial^2 T(z,t)}{\partial z^2} \tag{2}$$

where $t$ is the time, $z$ is the depth (positive upward), $T(z, t)$ is the temperature, and $\kappa$ is the soil thermal diffusivity defined as the soil thermal conductivity, $\lambda$, divided by the soil volumetric heat capacity, $c$ [*Jury et al.*, 1991]. When seasonal temperature variation at the ground surface ($z = 0$) is described by the following sinusoidal curve,

$$T(0,t) = A_0 \sin\left(\frac{2\pi}{\tau} t - \varphi\right) + T_{ave} \tag{3}$$

the amplitude of the annual soil temperature variation at depth $z$, $A(z)$, can be given by equation (2) as

$$A(z) = A_0 \exp\left(z\sqrt{\frac{\pi}{\tau\kappa}}\right) \tag{4}$$

where $A_0$ is the amplitude of annual temperature variation at the ground surface, $\tau$ is the period of the variation (= 365 d), $\phi$ is the lag of the phase, and $T_{ave}$ is the average annual temperature [*Jury et al.*, 1991]. Equation (4) can be transformed into the following equation:

$$\ln A(z) = \sqrt{\frac{\pi}{\tau\kappa}} \cdot z + \ln A_0 \tag{5}$$

Equation (5) indicates that ln $A(z)$ is linearly related to $z$ with a slope of $(\pi/\tau\kappa)^{1/2}$.

[45] We determined the value of $A$ at each measurement depth at point T by fitting a sinusoidal curve to the observed temperature variation (Figure 8; dashed lines). The ln $A$ value, calculated from the determined $A$ value, was plotted against $z$ in Figure 10. The figure demonstrates a strong linear relationship between ln $A$ and $z$ at this point, suggesting that the heat conduction processes at this point were little influenced by groundwater advection and that the value of $\kappa$ can be regarded as vertically homogeneous. The value of $\kappa$ at point T, calculated from the slope of the regression line for these data (Figure 10), was $5.8 \times 10^{-3}$ cm$^2$ s$^{-1}$.

#### 3.3.4.2. Soil Mantle Wells A–D

[46] Following the method applied to the temperature data at point T (Figure 8), we fitted a sinusoidal curve to the temperature data measured in wells A–D (Figures 9b–9e; dashed lines) to obtain the amplitude value $A$. Here, the fitting was done for the entire observation period for well A (Figure 9b), without SPG, and well C (Figure 9d), which always had SPG. For wells B (Figure 9c) and D (Figure 9e)

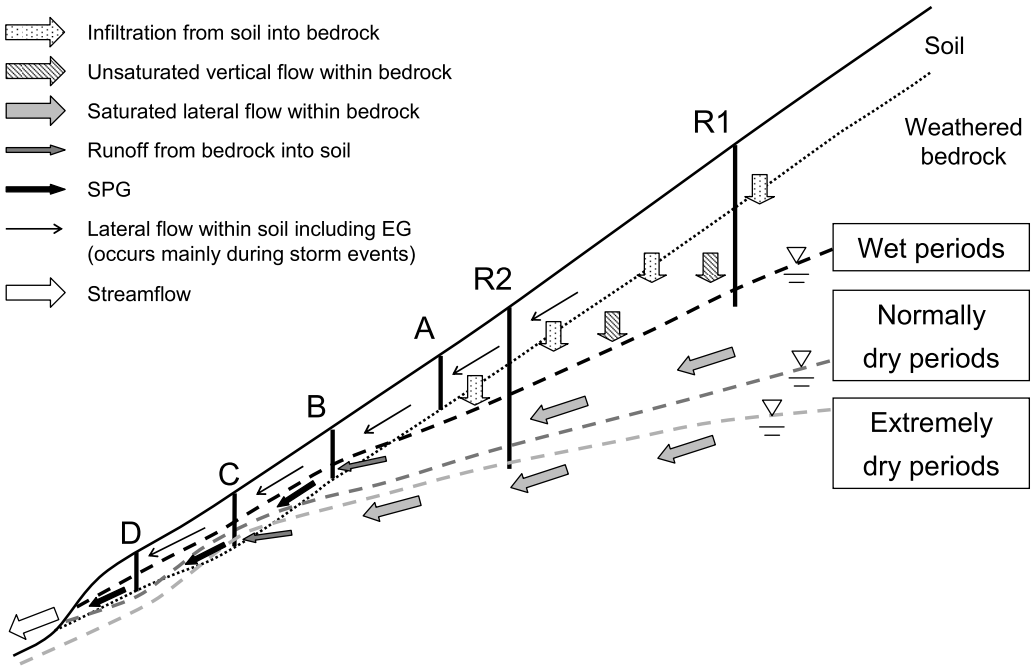


**Figure 11.** Schematic diagram of groundwater generation and water flow processes at the study site.

the fitting was carried out only for periods lacking SPG (indicated by red lines).

[47] Figure 10 shows the ($z$, ln $A$) data sets obtained for wells A–D together with point T data. The data points for wells A and B fell quite close to and on the regression line for the point T data, respectively, suggesting that the temperature variation at these points during periods without SPG is explained by the vertical thermal conduction process with the value of $\kappa$ assumed to be spatially homogeneous. This in turn indicates little influence of heat transport by groundwater advection on temperature variation at these points during periods without SPG, as was the case at point T.

[48] The data points for wells C and D, on the other hand, deviated downward from the point T regression line (Figure 10). Since the value of $\kappa$, which determines the slope of equation (5), can vary with varying water content, $\theta$ [*Jury et al.*, 1991], it is possible that the different $\theta$ condition at these two points from that at points T, A, and B created the deviation. Reports by *Tani et al.* [1979] and *Uchida et al.* [2003b] provide good estimates of the range of $\kappa$ for granitic soils. *Tani et al.* [1979] measured the annual soil temperature profile at five points in a granitic, forested headwater catchment located about 70 km east of our site and reported values of $\kappa$ ranging from $4.3 \times 10^{-3}$ to $8.0 \times 10^{-3}$ cm$^2$ s$^{-1}$. More recently, *Uchida et al.* [2003b] determined the value of $\kappa$ for granitic soils as $3.5 \times 10^{-3}$ cm$^2$ s$^{-1}$ using temperature data measured at seven points in a forested headwater catchment near the site of *Tani et al.* [1979]. Because these measurement points were located from at the ridge to near the channel, we assumed, based on their results, that the value of $\kappa$ for variously saturated granitic soils ranged from $3.5 \times 10^{-3}$ to $8.0 \times 10^{-3}$ cm$^2$ s$^{-1}$. This variation range of $\kappa$ ($= \lambda/c$) includes the value estimated for point T at our site ($5.8 \times 10^{-3}$ cm$^2$ s$^{-1}$) and seems reasonable because $c$ rises linearly with increasing $\theta$, whereas $\lambda$ exhibits its steepest rise in the low $\theta$ range, resulting in an internal maximum value of $\kappa$ as a function of $\theta$ and a relatively small range of $\kappa$ over a wide range of $\theta$ [*Jury et al.*, 1991]. The shaded area in Figure 10 displays the area delineated by two lines for equation (5), one given by the smallest $\kappa$ value ($3.5 \times 10^{-3}$ cm$^2$ s$^{-1}$) and the other by the largest $\kappa$ value ($8.0 \times 10^{-3}$ cm$^2$ s$^{-1}$), thus representing the possible data range that can be explained by the spatial variability of $\kappa$.

[49] Figure 10 demonstrates that the plot for well C still significantly deviated downward from the shaded area. This indicates that the thermal conduction equation (2) cannot explain the extremely small $A$ value for well C (depth: 130 cm). In general, when soil temperature varies without strong influence of groundwater advection, the value of $A$ is largest at the ground surface and decreases to zero with increasing depth, as observed at point T (Figures 8 and 10). The layer exhibiting no seasonal temperature variation (i.e., the value of $A$ is zero) is called the "isothermal layer" [*Arai*, 2004], and it is located 10 to 14 m below the ground surface in Japan [*Kiuchi*, 1950]. This was also the case at our site; the temperature in boreholes R1 (depth: 35 m, Figure 9f) and R2 (depth: 38 m, Figure 9g) varied only slightly between 11.4 and 12.8°C with no seasonal variation. This supports the conclusion that runoff of water stored in deep bedrock layers into soil layers generated SPG in the soil layers and diminished the $A$ value for well C. The SPG temperatures observed at points B (Figure 9c) and D (Figure 9e), which were similar to those at point C (Figure 9d) in both stability and value, can also be attributed to the effects of bedrock groundwater discharge.

[50] The data point for well D also fell beneath the shaded area (Figure 10), implying an influence of groundwater advection on temperature in well D. The cause of this

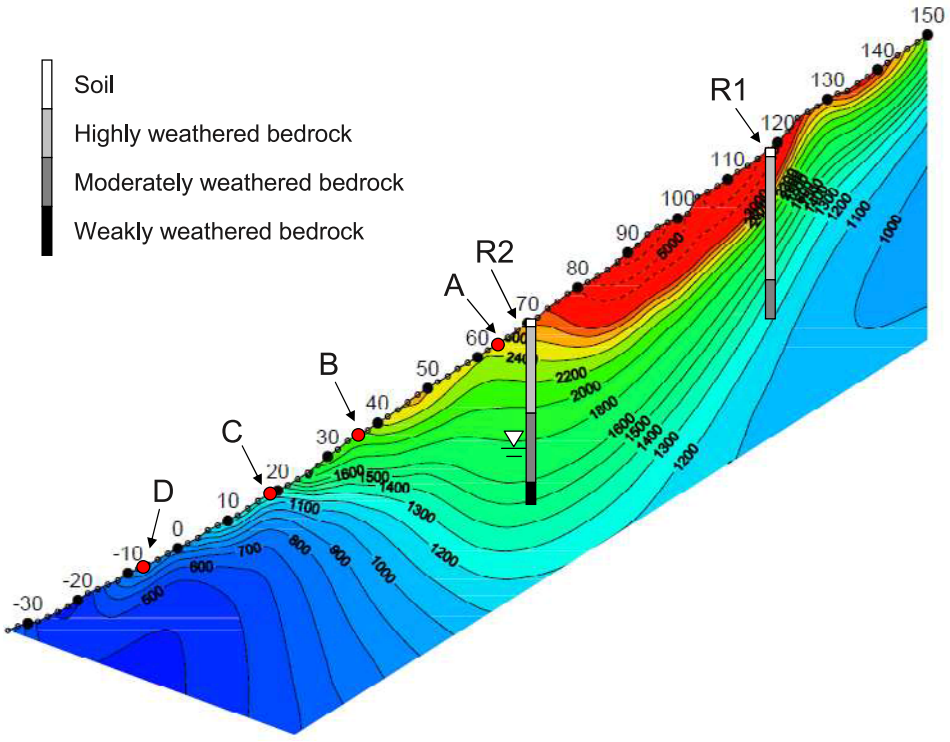


**Figure 12.** Resistivity [Ω m] profile observed on 18 February 2007. Groundwater levels of −26.4 m in borehole R2 and −112.9 cm in well C were observed on this date. Borehole R1 and the other soil mantle wells A, B, and D had no groundwater level. For boreholes R1 and R2, the observed weathering degrees are also shown.

deviation is discussed in more detail in the following section.

## 4. Discussion

### 4.1. Groundwater Generation and Water Flow Processes at the Study Site

#### 4.1.1. Upslope Areas (Point A)

[51] Based on the results and discussion above, Figure 11 schematically depicts groundwater generation and water flow processes at our site. At point A, groundwater was generated only during rainfall events and disappeared rapidly after the events ceased; i.e., only EG developed (Figure 3b). The EG dynamics showed no correlation with the bedrock groundwater level in borehole R2 (Figure 4a), and the $SiO_2$ concentrations of EG samples were very low (Figures 6b and 7). Moreover, the temperature in the well exhibited sinusoidal seasonal variation (Figure 9b), which was explained by heat conduction theory at a point with little influence of groundwater advection (Figure 10). These results indicate that soil mantle groundwater at point A was produced by the same mechanism conventionally used to explain hillslope hydrology; that is, rainwater infiltrating into and flowing downward in permeable soil layers reached the less permeable bedrock surface and formed an ephemeral saturated zone (i.e., EG) on the soil-bedrock interface (Figure 11). The contrasting values of saturated hydraulic conductivity between the soil ($1.2 \times 10^{-2} - 2.8 \times 10^{-1}$ cm $s^{-1}$) and the near-surface, highly weathered bedrock ($8.9 \times 10^{-5}$ and $2.9 \times 10^{-4}$ cm $s^{-1}$) support this. Since the groundwater level within the bedrock never rose to the level of point A, SPG never developed even in the wettest periods at this point (Figures 3b and 5). The absence of SPG generation in the upslope areas of our site was confirmed by long-term groundwater level monitoring conducted over three to seven years at eight points located above point A in the studied catchment [*Kosugi et al.*, 2002].

[52] The resistivity image profiling showed thick, unsaturated layers in upslope areas (Figure 12). In Figure 12, we present the resistivity profile of the study site on 18 February 2007. The figure displays a thick zone of extremely high resistivity in upslope areas including points R1, R2, and A. The core samples from boreholes R1 and R2 showed highly to moderately weathered bedrock with moderate saturated hydraulic conductivity values ($2.1 \times 10^{-6} - 3.4 \times 10^{-4}$ cm $s^{-1}$) for this zone (Figure 12). Because unsaturated granite with such high porosity exhibits extremely high resistivity [*Shima et al.*, 1995], the observed zone of high resistivity probably corresponded to highly weathered bedrock layers with little moisture. It can be presumed that unsaturated infiltration of water from the soil into such weathered bedrock was dominant in these upslope areas, consequently recharging groundwater within the bedrock (Figure 11).

#### 4.1.2. Middle-Slope Areas (Point B)

[53] At point B, runoff of bedrock groundwater into soil layers generated SPG in wet periods when the bedrock groundwater level rose; however, the SPG disappeared when the bedrock groundwater level fell. Thus, the development and disappearance of SPG, and the temporal variation in the SPG level, were closely related to groundwater level dynamics within the bedrock (Figures 3c, 3g, 4b, and

5). The low $SiO_2$ concentration of EG-alone-type groundwater (Figures 6c and 7) and the sinusoidal temperature variation during periods lacking SPG events (Figure 9c), the amplitude of which was as large as expected from the depth of well B with little influence of groundwater advection (Figure 10), indicate that point B was no longer influenced by deep bedrock groundwater when the bedrock groundwater level fell and therefore SPG was not generated. During such dry periods, EG was generated by the same mechanism operating at point A (Figure 11).

#### 4.1.3. Downslope Areas (Point C)

[54] At point C, SPG remained formed in soil layers by water discharged from deep bedrock throughout the observation period (Figures 3d and 5). Similar to point B, the SPG dynamics were synchronized with the bedrock groundwater dynamics (Figures 3d, 3g, and 4c). Hence, point C was always under the strong influence of deep bedrock groundwater not only with regard to groundwater level (Figures 3d and 4c) but also in groundwater chemistry (Figures 6d and 7) and temperature (Figures 9d and 10). Since SPG was always observed at point C, it follows that the groundwater level within the bedrock never fell below the level of point C even in dry periods (Figure 11).

[55] The core samples and the result of the resistivity image profiling (Figure 12) can help explain the occurrence of the saturated zone within bedrock above the level of point C even in the dry period. When resistivity image profiling was conducted on 18 February 2007, borehole R2 and well C had a bedrock groundwater level of −26.4 m and an SPG level of −112.9 cm, respectively, but borehole R1 and the other soil mantle wells A, B, and D showed no groundwater level, all suggesting dry catchment conditions on this date. Figure 12 displays the zone of low resistivity below the level of point C. The bedrock core samples taken from borehole R2 indicated the weakly weathered bedrock for this zone (depths below 33.5 m in R2; Figure 12). Because granite with low porosity and high saturation has low resistivity [*Shima et al.*, 1995], this low-resistivity zone probably represented weakly weathered, saturated bedrock layers. The saturated hydraulic conductivity of this zone, measured using the core sample, was $2.2 \times 10^{-9}$ cm $s^{-1}$. Existence of such weakly weathered bedrock layers with extremely low permeability may have caused the bedrock groundwater table to remain above the level of point C, the water flow to divert from vertical to lateral in direction, and SPG to occur in soil layers at point C throughout the year (Figure 11).

#### 4.1.4. Areas Near the Channel Head (Point D)

[56] At point D, SPG was also generated by runoff of bedrock groundwater into soil layers in the wet periods when the bedrock groundwater level rose (Figures 3e, 3g, 4d, and 5). During the dry periods without SPG generation, EG was generated in response to rainfall events (Figure 3e). Although such EG-alone-type groundwater observed at point D was very similar in waveform to that at points A and B, $SiO_2$ concentrations were considerably higher at the former than at the latter points (Figures 6 and 7). Moreover, while the $SiO_2$ concentration of the EG-with-SPG-type groundwater at the shallower depths at point B (Figure 6c) was often as low as that of the EG-alone-type groundwater (i.e., −60 and −50 cm on 29 September 2004, −60 to −40 cm on 20 October 2004, and −70 cm on 19 July 2006), the $SiO_2$ concentration at point D was characterized by relatively similar values throughout the well profile (Figure 6e). These results suggest a contribution of bedrock groundwater to EG $SiO_2$ concentrations at point D during storm events; since SPG, consisting of bedrock groundwater, always developed in the upper part of the slope (i.e., point C), rain or soil water could mix with such bedrock groundwater during storm events. Saturated lateral flow on the soil-bedrock interface would then have formed, flowing downslope to point D (Figure 11). During this process, rain or soil water likely mixed fully with the bedrock groundwater, causing the similar, relatively high $SiO_2$ concentrations of both EG-alone-type and EG-with-SPG-type groundwater throughout the profile at point D whether or not SPG developed at this point.

[57] Geothermal data (Figures 9e and 10), on the other hand, suggest an effect of bedrock groundwater on the temperature in well D in the dry periods without SPG generation. As shown in Figure 10, the data point for well D was plotted beneath the shaded area although the $A$ value for well D was determined for periods without SPG events. This suggests the influence of groundwater advection on temperature in well D even in dry periods when SPG was not generated. Careful examination of Figure 9 reveals that the agreement of the fitted sinusoidal curve to the observed temperature curve was slightly poorer for well D (Figure 9e) than for wells A (Figure 9b), B (Figure 9c), and C (Figure 9d). This was caused by the fact that the range of seasonal temperature variation during periods lacking SPG events was smaller in June 2004 through May 2005 (8.6–14.0°C) than in the following June 2005 through May 2006 (6.4–15.5°C), making the amplitude of the fitted sinusoidal curve (Figure 9e; dashed line) just the average value across the whole observation period.

[58] Figure 13 shows a detailed diagram of groundwater level dynamics and temperature variation in wells C and D. The entire observation period can be classified into three periods (wet, normally dry, and extremely dry periods) on the basis of the groundwater level in wells C (Figure 13b) and D (Figure 13c) and the temperature variation in well D (Figure 13c). In the wet periods (indicated by light blue backgrounds), SPG was generated in well D and the SPG level in well C was higher than approximately −100 cm. In the normally dry periods (pink backgrounds), no SPG was observed in well D, the SPG level in well C was between approximately −110 and −100 cm, and the amplitude of the observed temperature in well D was smaller than that of the fitted sinusoidal curve (dashed line in Figure 13c). In the extremely dry period (light orange backgrounds), no SPG was observed in well D, the SPG level in well C was lower than approximately −110 cm, and the amplitude of the observed temperature in well D was larger than that of the fitted sinusoidal curve (dashed line in Figure 13c). The figure demonstrates that both the highest and lowest seasonal temperatures in well D for June 2004 through May 2005 and for June 2005 through May 2006 were observed in the normally dry and extremely dry periods, respectively. For these two periods, we individually determined the $A$ value by calculating the difference between the highest and lowest temperature values (i.e., 5.4 and 9.1°C, respectively) and added these (ln $A$, $z$) data sets to Figure 10.

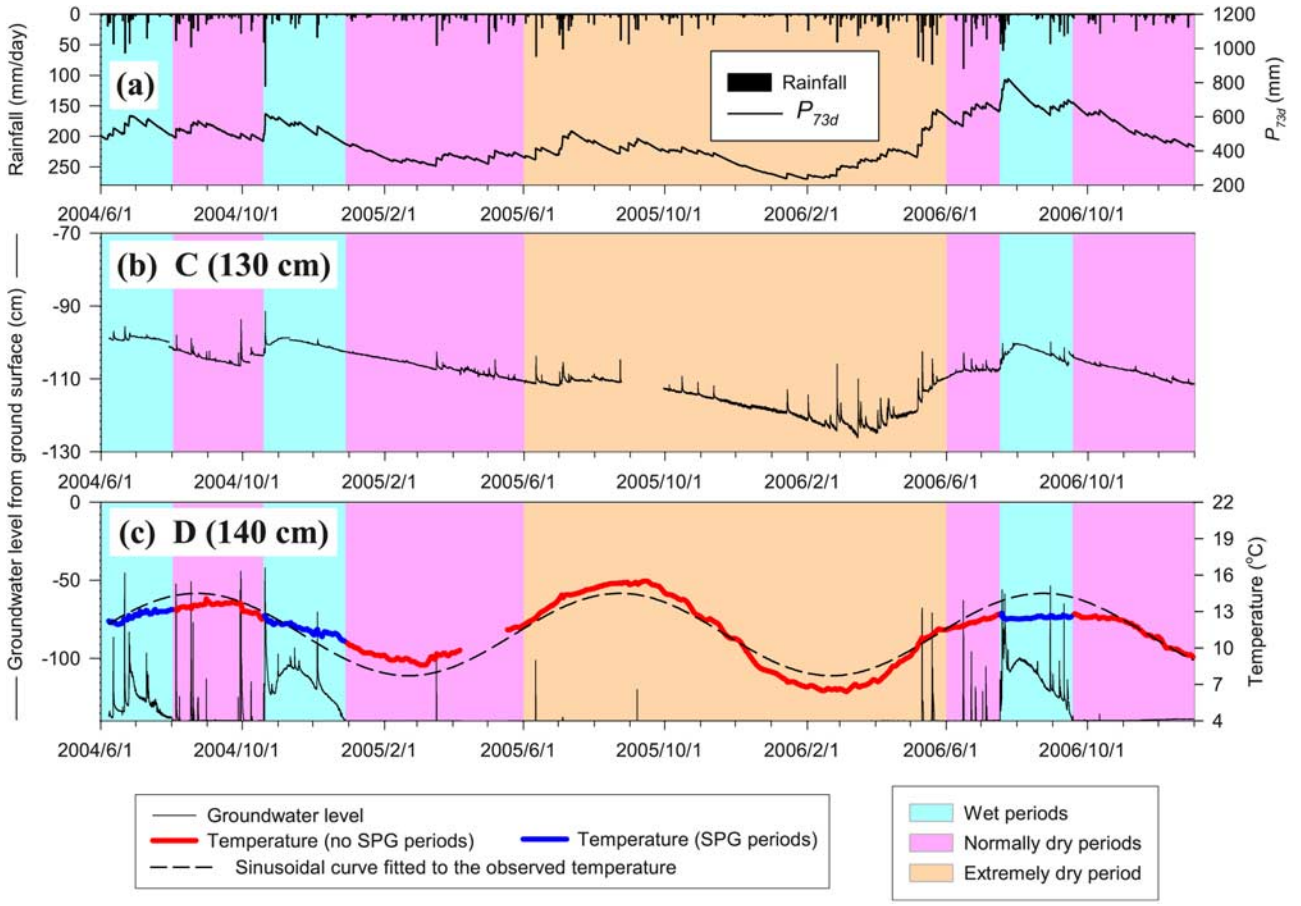


**Figure 13.** Detailed diagram of (a) rainfall and $P_{73d}$, (b) groundwater level in well C, and (c) groundwater level and temperature in well D. The sinusoidal curve fitted to the temperature variation observed during periods without SPG generation in well D is also shown in Figure 13c (dashed line). Light blue, pink, and light orange backgrounds indicate wet, normally dry, and extremely dry periods, respectively.

[59] The data point for June 2005 through May 2006 (an extremely dry period) fell on the lower edge of the shaded area. This suggests that the thermal conduction equation (2) with little influence of groundwater advection can consistently explain the $A$ value for this period, as at points A and B during periods without SPG. The data point for June 2004 through May 2005 (a normally dry period), on the other hand, is located further below the shaded area. Thus, the temperature variation at point D had different amplitude values depending on the catchment wetness.

[60] From the results and discussion above, we can infer the following mechanism controlling the temperature variation in well D. Even during the dry periods when SPG disappeared from the soil layers and was no longer observed in well D, bedrock groundwater, the $A$ value of which was very small, flowed in relatively shallow bedrock layers, affecting the temperature at the bottom of well D for a long time. In extremely dry periods, the groundwater level, which was "hidden" in the shallow bedrock, was also low compared to the normally dry periods. This probably caused the "hidden" shallow bedrock groundwater flow, which could affect the temperature in well D in the normally dry periods, to lose its influence, as was observed at point B (Figure 11).

[61] Whereas point C never "hid" the bedrock groundwater once discharged into soil layers (i.e., SPG was observed throughout the observation period), groundwater discharged from the bedrock into soil layers was often "hidden" in shallow bedrock layers at point D (Figures 3d and 3e). This led to the apparently mysterious phenomenon of the absence of SPG at point D even in the period of SPG generation at point C, which is located above point D. The difference may be attributed to different bedrock properties around these points. From the large spatial variability in bedrock permeability and the patchily distributed saturated area in the soil layers during natural or applied rainfall events, *Wilson and Dietrich* [1987], *Montgomery et al.* [1997], and *Montgomery et al.* [2002] inferred that a block of bedrock with low permeability forced bedrock groundwater to exfiltrate into soil layers. The apparently inconsistent groundwater dynamics observed at points C and D at our site may be explained by a similar mechanism; the low permeability of surface bedrock around point C kept bedrock groundwater, once discharged into soil layers in the upper slope, flowing in the soil layers, whereas the relatively high permeability of surface bedrock at point D, probably derived from more fractures and/or the higher weathering degree, allowed infiltration back into bedrock layers (Figure 11).

[62] Results of the resistivity image profiling (Figure 12) support the inference above. No groundwater was observed in well D, but in well C an SPG level of −112.9 cm was detected when the resistivity image profiling was carried out on 18 February 2007, suggesting extremely dry catchment conditions on this date. As shown in Figure 12, whereas the low-resistivity zone bulged up near to the surface just upslope of point D, the shallow, near-surface layers at point D exhibited relatively high resistivity. Since higher resistivity signifies materials with higher porosity and lower saturation [*Shima et al.*, 1995], this higher-resistivity zone over the surface layer around point D implies the existence of relatively thick, weathered, and unsaturated bedrock layers with high porosity. This agrees well with the inference above that the bedrock at point D may contain more fractures and/or be more weathered.

### 4.2. Importance of Direct Measurements of Conditions Within Bedrock

[63] Although previous studies have emphasized the contribution of bedrock groundwater to groundwater generation or pressure head responses in soil layers, such suggestions were generally based on hydrologic, hydrochemical, and thermal observations of soil layers and streamflow [e.g., *McGlynn et al.*, 1999; *Uchida et al.*, 2003a, 2003b; *Hattanji and Onda*, 2004] or piezometric and tensiometric measurements within bedrock [e.g., *Wilson and Dietrich*, 1987; *Montgomery et al.*, 1997]. These studies also lacked data on the bedrock condition or only provided flow direction analyses based on pressure head records, making it difficult to directly verify the inferences. However, by directly measuring the groundwater level (Figure 3), groundwater chemistry (Figure 6), and temperature (Figure 9) within the bedrock, this study has clearly demonstrated the effects of bedrock groundwater on soil mantle groundwater dynamics (Figure 11). Moreover, this study has revealed that groundwater discharged from the bedrock into the soil layers (i.e., SPG) exhibited different dynamics at points B, C, and D (Figures 3c–3e) within the small headwater catchment studied. No previous studies have reported such phenomena because few long-term observations using multiple soil mantle wells installed in areas where bedrock groundwater exfiltrates into soil layers have been conducted. Here, the direct and detailed measurements of groundwater level, chemistry, and temperature in the bedrock, taken together within soil layers, have revealed that the apparently distinct SPG dynamics, including generations and disappearances, observed at points B, C, and D were controlled by groundwater level dynamics within the bedrock (Figures 3–5), leading to different effects on the soil mantle groundwater chemistry (Figures 6 and 7) and temperature (Figures 9 and 10) at each point in the catchment (Figure 11). This study emphasizes the importance of direct measurements of conditions within the bedrock, such as the groundwater level, chemistry, and temperature, to clarify the roles of bedrock in hydrological and hydrochemical processes in headwater catchments.

## 5. Conclusions

[64] Detailed observations conducted in a granitic headwater catchment in central Japan revealed two types of soil mantle groundwater generation in this catchment: (1) groundwater that developed in response to rainfall events and disappeared rapidly after the events ceased (EG), and (2) groundwater that remained formed for more than several months (SPG). The development, dynamics, and disappearance of SPG were closely related to groundwater level dynamics within the deep bedrock. Moreover, the $SiO_2$ concentrations of the SPG were much higher than those of the EG and as high as those of deep bedrock groundwater. Furthermore, the SPG maintained a relatively constant temperature of approximately 12°C, which could be explained not by the sinusoidal seasonal variation of the soil temperature at a point where groundwater advection exerted minimal effects on temperature, but by the temperature of the deep bedrock layers that exhibited no seasonal variation. All of these results indicate that runoff of bedrock groundwater into soil layers generates SPG, whereas EG consists of water flowing only through soil layers.

[65] The groundwater generation processes in soil layers in the catchment varied both spatially and temporally under the influence of the underlying bedrock. Only EG was generated in the upslope areas (point A), where recharge of deep bedrock groundwater was expected to dominantly occur. The recharged bedrock groundwater continuously exfiltrated into overlying soil layers in the downslope areas (point C), forming SPG throughout the year. In the middle-slope areas (point B), SPG was generated in the wet periods when the groundwater level within deep bedrock rose and disappeared in the dry periods when the bedrock groundwater level fell. Thus, bedrock groundwater dynamics determined the timing, location, and level of SPG generation within soil layers. In areas near the channel head (point D), we inferred that groundwater coming from deep bedrock layers always flowed in the relatively shallow bedrock layers even in dry periods when SPG disappeared from the soil layers probably due to the higher permeability of the surface bedrock. Both the degree of weathering and the permeability of core samples taken from the boreholes and the results of the resistivity image profiling were consistent with the groundwater generation and water flow processes of the study site described above.

[66] This study has clarified the effects of bedrock on the spatial and temporal variations in soil mantle groundwater by directly measuring the groundwater level, chemistry, and temperature within the bedrock. It has also shown that direct measurement of conditions within the bedrock is important to elucidate the effects of bedrock on various phenomena occurring in headwater catchments. Another important implication of this study, regarding the development of physically based models of water flow processes and landslides occurrence, is that groundwater generation processes in soil layers cannot be determined primarily by soil or bedrock surface topography. Rather, such processes are strongly affected by groundwater dynamics within the bedrock. This, in turn, suggests that further improvement of the accuracy of hydrological and landslide-prediction models requires incorporation of the effects of the underlying bedrock. Furthermore, bedrock groundwater exfiltration elevated $SiO_2$ concentrations and damped subsurface temperature variation, implying that bedrock groundwater contributes to stream water chemistry and biogeochemical processes. Future work should particularly investigate water flow processes within bedrock, which are still poorly

understood, to clarify the roles of bedrock in hydrological, hydrochemical, and biogeochemical phenomena and in the occurrence of landslides in headwater catchments.

[67] **Acknowledgments.** We thank two anonymous reviewers for their helpful comments. We also thank T. Hirokawa, S. Yamashita, and Y. Sako for their support in the drilling and resistivity image profiling. This study was partly supported by a grant from the Rokko Sabo Office, Kinki Division, Ministry of Land, Infrastructure and Transport, Japan; the River Fund in charge of the Foundation of River and Watershed Environment Management (FOREM), Japan; and a grant from the Fund of Monbusho for Scientific Research (19380087, 19-5131).

## References

Anderson, S. P., W. E. Dietrich, D. R. Montgomery, R. Torres, M. E. Conrad, and K. Loague (1997), Subsurface flow paths in a steep, unchanneled catchment, *Water Resour. Res.*, *33*, 2637–2653, doi:10.1029/97WR02595.

Arai, T. (2004), *Hydrology for Regional Analysis* (in Japanese), 309 pp., Kokon Shoin, Tokyo.

Asano, Y., T. Uchida, and N. Ohte (2003), Hydrologic and geochemical influences on the dissolved silica concentration in natural water in a steep headwater catchment, *Geochim. Cosmochim. Acta*, *67*(11), 1973–1989, doi:10.1016/S0016-7037(02)01342-X.

Bazemore, D. E., K. N. Eshleman, and K. J. Hollenbeck (1994), The role of soil water in stormflow generation in a forested headwater catchment: Synthesis of natural tracer and hydrometric evidence, *J. Hydrol. Amsterdam*, *162*, 47–75, doi:10.1016/0022-1694(94)90004-3.

Beven, K. J., and M. J. Kirkby (1979), A physically based, variable contributing area model of basin hydrology, *Hydrol. Sci. Bull.*, *24*(1), 43–69.

Burns, D. A., P. S. Murdoch, G. B. Lawrence, and R. L. Michel (1998), Effect of groundwater springs on $NO_3^-$ concentrations during summer in Catskill Mountain streams, *Water Resour. Res.*, *34*, 1987–1996, doi:10.1029/98WR01282.

Downer, C. W., and F. L. Ogden (2004), GSSHA: Model to simulate diverse stream flow producing processes, *J. Hydrol. Eng.*, *9*, 161–174, doi:10.1061/(ASCE)1084-0699(2004)9:3(161).

Everett, A. G. (1979), Secondary permeability as a possible factor in the origin of debris avalanches associated with heavy rainfall, *J. Hydrol. Amsterdam*, *43*, 347–354, doi:10.1016/0022-1694(79)90180-X.

Frazier, C. S., R. C. Graham, P. J. Shouse, M. V. Yates, and M. A. Anderson (2002), A field study of water flow and virus transport in weathered granitic bedrock, *Vadose Zone J.*, *1*, 113–124.

Grayson, R. B., I. D. Moore, and T. A. McMahon (1992), Physically based hydrologic modeling 1. A terrain-based model for investigative purposes, *Water Resour. Res.*, *28*, 2639–2658, doi:10.1029/92WR01258.

Haria, A. H., and P. Shand (2004), Evidence for deep sub-surface flow routing in forested upland Wales: Implications for contaminant transport and stream flow generation, *Hydrol. Earth Syst. Sci.*, *8*, 334–344.

Hattanji, T., and Y. Onda (2004), Coupling of runoff processes and sediment transport in mountainous watersheds underlain by different sedimentary rocks, *Hydrol. Process.*, *18*, 623–636, doi:10.1002/hyp.1262.

Hendrayanto, , K. Kosugi, T. Uchida, S. Matsuda, and T. Mizuyama (1999), Spatial variability of soil hydraulic properties in a forested hillslope, *J. For. Res.*, *4*, 107–114, doi:10.1007/BF02762234.

Jury, W. A., W. R. Gardner, and W. H. Gardner (1991), *Soil Physics*, pp. 159–195, Wiley, New York.

Katsura, S., K. Kosugi, N. Yamamoto, and T. Mizuyama (2006), Saturated and unsaturated hydraulic conductivities and water-retention characteristics of weathered granitic bedrock, *Vadose Zone J.*, *5*, 35–47, doi:10.2136/vzj2005.0040.

Katsuyama, M., N. Ohte, and N. Kabeya (2005), Effects of bedrock permeability on hillslope and riparian groundwater dynamics in a weathered granite catchment, *Water Resour. Res.*, *41*, W01010, doi:10.1029/2004WR003275.

Kiuchi, S. (1950), The study of climate under the ground: The observation on the depth and temperature of isothermal stratum in Japan & Manchuria (in Japanese with English abstract), *J. Geog.*, *677*, 88–92.

Kosugi, K., T. Mizuyama, and M. Fujita (2002), Accuracy of a shallow-landslide prediction model to estimate groundwater table (in Japanese with English abstract), *J. Jpn. Soc. Erosion Control Eng.*, *55*(3), 21–32.

Kosugi, K., S. Katsura, M. Katsuyama, and T. Mizuyama (2006), Water flow processes in weathered granitic bedrock and their effects on runoff generation in a small headwater catchment, *Water Resour. Res.*, *42*, W02414, doi:10.1029/2005WR004275.

Kosugi, K., S. Katsura, T. Mizuyama, S. Okunaka, and T. Mizutani (2008), Anomalous behavior of soil mantle groundwater demonstrates the major effects of bedrock groundwater on surface hydrological processes, *Water Resour. Res.*, *44*, W01407, doi:10.1029/2006WR005859.

Legout, C., J. Molenat, L. Aquilina, C. Gascuel-Odoux, M. Faucheux, Y. Fauvel, and T. Bariac (2007), Solute transfer in the unsaturated zone-groundwater continuum of a headwater catchment, *J. Hydrol. Amsterdam*, *332*, 427–441, doi:10.1016/j.jhydrol.2006.07.017.

McDonnell, J. J. (1990), A rationale for old water discharge through macropores in a steep, humid catchment, *Water Resour. Res.*, *26*, 2821–2832.

McGlynn, B. L., J. J. McDonnell, J. B. Shanley, and C. Kendall (1999), Riparian zone flowpath dynamics during snowmelt in a small headwater catchment, *J. Hydrol. Amsterdam*, *222*, 75–92, doi:10.1016/S0022-1694(99)00102-X.

Montgomery, D. R., and W. E. Dietrich (1994), A physically based model for the topographic control on shallow landsliding, *Water Resour. Res.*, *30*, 1153–1171, doi:10.1029/93WR02979.

Montgomery, D. R., W. E. Dietrich, R. Torres, S. P. Anderson, J. T. Heffner, and K. Loague (1997), Hydrologic response of a steep, unchanneled valley to natural and applied rainfall, *Water Resour. Res.*, *33*, 91–109, doi:10.1029/96WR02985.

Montgomery, D. R., W. E. Dietrich, and J. T. Heffner (2002), Piezometric response in shallow bedrock at CB1: Implications for runoff generation and landsliding, *Water Resour. Res.*, *38*(12), 1274, doi:10.1029/2002WR001429.

Mosley, M. P. (1979), Streamflow generation in a forested watershed, New Zealand, *Water Resour. Res.*, *15*, 795–806, doi:10.1029/WR015i004p00795.

Mosley, M. P. (1982), Subsurface flow velocities through selected forest soils, South Island, *N.Z. J. Hydrol.*, *55*, 65–92, doi:10.1016/0022-1694(82)90121-4.

Mulholland, P. J. (1993), Hydrometric and stream chemistry evidence of three storm flowpaths in Walker Branch Watershed, *J. Hydrol. Amsterdam*, *151*, 291–316, doi:10.1016/0022-1694(93)90240-A.

Noguchi, S., Y. Tsuboyama, R. C. Sidle, and I. Hosoda (1999), Morphological characteristics of macropores and the distribution of preferential flow pathways in a forested slope segment, *Soil Sci. Soc. Am. J.*, *63*, 1413–1423.

Okimura, T., and R. Ichikawa (1985), A prediction method for surface failures by movements of infiltrated water in a surface soil layer, *Nat. Disaster Sci.*, *7*, 41–51.

O'Loughlin, E. M. (1986), Prediction of surface saturation zones in natural catchments by topographic analysis, *Water Resour. Res.*, *22*, 794–804, doi:10.1029/WR022i005p00794.

Onda, Y., Y. Komatsu, M. Tsujimura, and J. Fujihara (1999), Possibility for predicting landslide occurrence by analyzing the runoff peak response time, (in Japanese), *J. Jpn. Soc. Erosion Control Eng.*, *51*(5), 48–52.

Peters, D. L., J. M. Buttle, C. H. Taylor, and B. D. LaZerte (1995), Runoff production in a forested, shallow soil, Canadian Shield basin, *Water Resour. Res.*, *31*, 1291–1304, doi:10.1029/94WR03286.

Rosso, R., M. C. Rulli, and G. Vannucchi (2006), A physically based model for the hydrologic control on shallow landsliding, *Water Resour. Res.*, *42*, W06410, doi:10.1029/2005WR004369.

Scanlon, T. M., J. P. Raffensperger, and G. M. Hornberger (2001), Modeling transport of dissolved silica in a forested headwater catchment: Implications for defining the hydrochemical response of observed flow pathways, *Water Resour. Res.*, *37*, 1071–1082, doi:10.1029/2000WR900278.

Shima, H., K. Kajima, and H. Kamiya (1995), *Resistivity Image Profiling* (in Japanese), 206 pp., Kokon Shoin, Tokyo.

Shimada, Y., N. Ohte, N. Tokuchi, and M. Suzuki (1992), $SiO_2$ concentration of groundwater and streamwater in a small forested watershed (in Japanese with English abstract), *J. Jpn. Soc. Hydrol. Water Resour.*, *5*, 3–11.

Sklash, M. G., M. K. Stewart, and A. J. Pearce (1986), Storm runoff generation in humid headwater catchments: 2. A case study of hillslope and low-order stream response, *Water Resour. Res.*, *22*, 1273–1282, doi:10.1029/WR022i008p01273.

Soulsby, C. (1992), Hydrological controls on acid runoff generation in an afforested headwater catchment at Llyn Brianne, Mid-Wales, *J. Hydrol. Amsterdam*, *138*, 431–448, doi:10.1016/0022-1694(92)90129-J.

Soulsby, C., D. Tetzlaff, N. van den Bedem, I. A. Malcolm, P. J. Bacon, and A. F. Youngson (2007), Inferring groundwater influences on surface water in montane catchments from hydrochemical surveys of springs and streamwaters, *J. Hydrol. Amsterdam*, *333*, 199–213, doi:10.1016/j.jhydrol.2006.08.016.

Suzuki, M., and S. Kobashi (1981), The critical rainfall for the disasters caused by slope failures (in Japanese with English abstract), *Shin Sabo*, *121*, 16–26.

Tani, M. (1997), Runoff generation processes estimated from hydrological observations on a steep forested hillslope with a thin soil layer, *J. Hydrol. Amsterdam*, *200*, 84–109, doi:10.1016/S0022-1694(97)00018-8.

Tani, M., Y. Fukushima, and M. Suzuki (1979), Annual variation of soil temperature in a small mountain watershed (in Japanese with English abstract), *Bull. Kyoto Univ. For.*, *51*, 138–151.

Terajima, T., A. Mori, and H. Ishii (1993), Comparative study of deep percolation amount in two small catchments in granitic mountain (in Japanese with English abstract), *Jpn. J. Hydrol. Sci.*, *23*(2), 105–118.

Tsuboyama, Y., R. C. Sidle, S. Noguchi, S. Murakami, and T. Shimizu (2000), A zero-order basin—Its contribution to catchment hydrology and internal hydrological processes, *Hydrol. Process.*, *14*, 387–401, doi:10.1002/(SICI)1099-1085(20000228)14:3<387::AID-HYP944>3.0.CO;2-Q.

Uchida, T., Y. Asano, N. Ohte, and T. Mizuyama (2003a), Analysis of flowpath dynamics in a steep unchannelled hollow in the Tanakami Mountains of Japan, *Hydrol. Process.*, *17*, 417–430, doi:10.1002/hyp.1133.

Uchida, T., Y. Asano, N. Ohte, and T. Mizuyama (2003b), Seepage area and rate of bedrock groundwater discharge at a granitic unchanneled hillslope, *Water Resour. Res.*, *39*(1), 1018, doi:10.1029/2002WR001298.

VanderKwaak, J. E., and K. Loague (2001), Hydrologic-response simulations for the R-5 catchment with a comprehensive physics-based model, *Water Resour. Res.*, *37*, 999–1013, doi:10.1029/2000WR900272.

Wigmosta, M. S., and S. J. Burges (1997), An adaptive modeling and monitoring approach to describe the hydrologic behavior of small catchments, *J. Hydrol. Amsterdam*, *202*, 48–77, doi:10.1016/S0022-1694(97)00057-7.

Wilson, C. J., and W. E. Dietrich (1987), The contribution of bedrock groundwater flow to storm runoff and high pore pressure development in hollows, *IAHS Publ.*, *165*, 49–59.

Wilson, G. V., P. M. Jardine, J. D. O'Dell, and M. Collineau (1993), Field-scale transport from a buried line source in variably saturated soil, *J. Hydrol. Amsterdam*, *145*, 83–109, doi:10.1016/0022-1694(93)90221-T.

Wu, W., and R. C. Sidle (1995), A distributed slope stability model for steep forested basins, *Water Resour. Res.*, *31*, 2097–2110, doi:10.1029/95WR01136.

Yokoyama, T., Y. Sato, Y. Maeda, T. Tarutani, and P. Maeda (1993), Siliceous deposits formed from geothermal water. I. The major constituents and the existing states of iron and aluminum, *Geochem. J.*, *27*, 375–384.

S. Katsura, K. Kosugi, T. Mizutani, T. Mizuyama, and S. Okunaka, Laboratory of Erosion Control, Department of Forest Science, Graduate School of Agriculture, Kyoto University, Kitashirakawa Oiwakecho, Kyoto 606-8502, Japan. (katsura3@kais.kyoto-u.ac.jp)